HHS Public Access

Author manuscript

Nat Cell Biol. Author manuscript; available in PMC 2018 December 18.

Published in final edited form as:

Nat Cell Biol. 2018 July ; 20(7): 823–835. doi:10.1038/s41556-018-0126-z.

AMP Kinase Promotes Glioblastoma Bioenergetics and Tumor Growth

Rishi Raj Chhipa[1], **Qiang Fan**[1], **Jane Anderson**[1], **Ranjithmenon Muraleedharan**[1], **Yan Huang**[2], **Georgianne Ciraolo**[3], **Xiaoting Chen**[6], **Ronald Waclaw**[4], **Lionel M. Chow**[1], **Zaza Khuchua**[2,$], **Matthew Kofron**[5], **Matthew T. Weirauch**[6,5], **Ady Kendler**[7], **Christopher McPherson**[8], **Nancy Ratner**[4], **Ichiro Nakano**[9], **Nupur Dasgupta**[10], **Kakajan Komurov**[4], and **Biplab Dasgupta**[1,*]

[1]Division of Oncology, Cincinnati Children's Hospital Medical Center, Cincinnati, OH

[2]Division of Molecular and Cardiovascular Biology, Cincinnati Children's Hospital Medical Center, Cincinnati, OH

[3]Division of Pathology and Laboratory Medicine, Cincinnati Children's Hospital Medical Center, Cincinnati, OH

[4]Division of Experimental Hematology and Cancer Biology, Cincinnati Children's Hospital Medical Center, Cincinnati, OH

[5]Division of Developmental Biology, Cincinnati Children's Hospital Medical Center, Cincinnati, OH

[6]Division of Center for Autoimmune Genomics and Etiology and Biomedical Informatics, Cincinnati, OH

[7]Department of Pathology and Laboratory Medicine, University of Cincinnati, OH

[8]Department of Neurosurgery, Brain Tumor Center, University of Cincinnati Neuroscience Institute and Mayfield Clinic, Cincinnati, OH

[9]Department of Neurosurgery, University of Alabama

[10]Division of Human Genetics, Cincinnati Children's Hospital Medical Center, Cincinnati, OH

Abstract

Stress is integral to tumor evolution, and cancer cell survival depends on stress management. We found that cancer-associated stress chronically activate the bioenergetic sensor AMP kinase (AMPK), and tumor cells hijack an AMPK-regulated stress response pathway conserved in normal cells, to survive. Analysis of The Cancer Genome Atlas (TCGA) data revealed that AMPK isoforms are highly expressed in the lethal human cancer Glioblastoma (GBM). We show that AMPK inhibition reduces viability of patient-derived GBM stem cells (GSCs) and tumors. In stressed (exercised) skeletal muscle, AMPK is activated to cooperate with the cAMP response

[*]**Corresponding Author, Contact**: Biplab Dasgupta PhD, Associate Professor of Pediatrics, Division of Oncology, Cincinnati Children's Hospital Medical Center, 3333 Burnet Avenue, Cincinnati OH 45229, Biplab.dasgupta@cchmc.org, Phone: 513-8031370.
[$]Current affiliation: Sechenov University, Department of Biochemistry. Moscow, Russian Federation.

element binding protein-1 (CREB1) and promote glucose metabolism. We demonstrate that oncogenic stress chronically activates AMPK in GSCs that coopt the AMPK-CREB1 pathway to coordinate tumor bioenergetics through the transcription factors HIF1α and GABPA. Finally, we show that adult mice tolerate systemic deletion of AMPK supporting the utility of AMPK pharmacological inhibitors in the treatment of GBM.

The serine-threonine kinase AMPK is a heterotrimeric protein complex of catalytic α, and regulatory β and γ subunits[1–3]. All AMPK subunits are required for AMPK stability and activity[4]. At lower cellular energy state the γ subunits bind AMP/ADP and enhance AMPK activity to bring about energy homeostasis. AMP/ADP binding also enables the upstream metabolic kinases LKB1 and CAMKKβ to phosphorylate α subunits, fully activating AMPK[5, 6]. AMPK is a metabolic hub[1–3], yet its function in cancer cell metabolism remains undefined. AMPK inhibits biosynthetic kinases like mammalian target of rapamycin (mTOR) and acetyl Co-A carboxylase (ACC) [7–9]. Therefore, AMPK is expected to play a suppressive role in cancer. Despite its tumor suppressive role in other cancers[10], a potential oncogenic role of activated AMPK was alluded in astrocytic tumors of the brain[11]. Controversy surrounding its role in cancer stems in part due to the absence of genetic models and use of non-specific pharmacological agents[12]. Contrary to the early pharmacological studies [13–16], some recent genetic studies showed that in some contexts, AMPK provides survival advantage critical for tumor growth[17–22]. In contrast, AMPKα1 knockout enhanced glycolysis and accelerated tumorigenesis in a lymphoma mouse model[10], demonstrating species-specific and tissue-specific effects. Glycolysis is positively regulated by HIF1α. The role of AMPK in glycolysis and its relation with HIF1α is however unclear. HIF1α that is degraded in the presence of O_2 was found to be stabilized under normoxic condition in LKB1 deficient MEFS (where AMPK activity is reduced)[23]. In contrast, no such HIF1α stabilization was observed in AMPK null MEFs[21]. While AMPK was found to inhibit Warburg effect through HIF1α destabilization in mouse lymphoma[10] and reduce glycolysis in mouse ALL[24], AMPK promoted glycolysis in mitotically stressed cells, breast tumors, skin fibroblasts and astrocytes[17, 25–28]. In this study, we present a mechanism by which AMPK regulates HIF1α transcription and glycolysis in GBM. We provide evidence that through phosphorylation of CREB1, a transcription factor highly expressed in GBM, AMPK controls HIF1α and GABPA transcription to regulate GBM bioenergetics.

RESULTS

AMPK is highly expressed in GBM

While querying the TCGA database for differentially expressed metabolic kinases in human cancer, we observed significantly higher expression of AMPK α1, β1 and γ1 subunits; $p \leq 10^{-7}$) in GBM than normal brain (Fig. 1a), and in GBM relative to lower grade glioma (LGG) (Fig. 1b; $p \leq 10^{-14}$). Higher expression of AMPKα1 ($p = 0.0007$), β1 ($p = 0.01$), pAMPK (active AMPK, $p = 0.003$) and AMPK substrate pACC ($p = 0.01$) also correlated with poor patient survival in LGG (Fig. 1c, Supplementary Fig. 1a), but not with GBM (Supplementary Fig. 1b), potentially due to higher basal expression of AMPK across all GBM relative to LGG. This is reminiscent of other genes (e.g., HIF1α, CREB1) that are

highly expressed, sometimes uniformly across GBM relative to LGG[29–31], but also not prognostic, yet important for GBM pathogenesis[32–34]. Biochemical analysis of human GBM and mouse high-grade glioma (HGG)[12, 35] (Fig. 1d–g; Supplementary Fig. 1c) revealed that active (phosphorylated) AMPK is high in tumors compared to normal brain tissue, and higher in tumor cells relative to infiltrating macrophages (Supplementary Fig. 1d, e). Compared to normal brain, AMPK upstream kinases CAMKKβ and LKB1 were not upregulated (Fig. 1d). Of the AMPK subunits, the α and β but not γ1 were upregulated in GBM (Fig. 1d). The high pAMPK signature was retained in primary GBM stem cell lines (GSCs) derived from fresh tumor tissue of both proneural and mesenchymal subtypes (Fig. 1h).

In normal cells, glucose starvation activates, while glucose feeding diminishes AMPK activity [1–3]. Remarkably, unlike normal human glial cells the high AMPK activity in GSCs was chronically maintained and was insensitive to glucose levels, (Fig. 1i). We questioned if high AMPK activity is due to oncogenesis-associated stress (OAS). OAS constitutes a variety of stress signals including ER stress, DNA damage response, oxidative stress etc. that are elicited in response to and to cope with oncogenic events[36]. GBM demonstrated high genotoxic and ER stress relative to normal brain cells and tissue (Supplementary Fig. 1f–h). Agents that mimicked OAS (Supplementary Fig. 1i, j) also activated AMPK (Supplementary Fig. 1k–m), suggesting a link between OAS and active AMPK in GBM. Consistent with this observation, expression of oncogenic EGFR or KRAS, or reducing PTEN levels in detached human astrocytes increased AMPK phosphorylation (Supplementary Fig. 1n–p).

AMPK is required for viability of patient-derived primary GSCs

We interrogated if pAMPK is merely an indicator of OAS or necessary for viability of GSCs. AMPK silencing by AMPKβ1 shRNA induced apoptosis (Fig 1j; Supplementary Video 1a, b). Depletion of AMPK by five independent genetic strategies (two AMPKβ1 shRNAs, three β1 siRNAs, dominant negative AMPKα2, AMPKα1α2 shRNAs and AMPKβ1 CRISPR) significantly reduced (~40–70%) viability of primary GSC lines; normal human astrocytes (NHA) remained relatively viable (Fig. 1k; Fig. 2a–h). Cre-mediated deletion of AMPKβ1 also reduced viability of oncogenic mouse neural stem cells (NPCs) (Fig. 2i). Strikingly, viability of long-established GBM serum lines U87, A172 and T98G remained unaffected by AMPK shRNA (Fig. 2j). The effect of human AMPKβ1 shRNA was specific because, expression of shRNA-resistant mouse AMPKβ1 cDNA in GSC9 and 10 lines rescued viability defects (Fig. 2k, l). Consistent with a previous report [37], the AMPK β1 subunit was specifically critical for survival, because depletion of the less expressed β2 subunit did not reduce pAMPK levels or induce cell death, and its overexpression failed to rescue β1-silenced cells (Fig. 2m–o). Inhibition of upstream kinases that activate AMPK (LKB1 and CAMKKβ) also reduced viability of GSC lines, consistent with the AMPK activation pathway being important for GBM (Fig. 2p).

AMPK activation during metabolic and oncogenic stress provides protection[36]. Yet unexpectedly, a tumor-mimetic metabolic stress-like condition (1mM glucose or 1% O_2), did not enhance death of AMPK-silenced GSCs beyond what occurred at physiologically relevant 5mM glucose at which our primary GSC lines are grown (Fig. 2q). In fact, unlike

long-established GBM serum lines, primary GSCs remained viable under stress (Fig. 2q, r). Thus, stress-tolerant primary lines are reliable surrogates of the tumor in maintaining an AMPK-dependent stress adaptation mechanism for survival *in vitro*.

AMPK is required for intracranial growth of GSC-derived tumors

To test if AMPK is necessary for tumor growth *in vivo*, we transplanted four primary GSC lines expressing nontarget control (NT) or AMPKβ1shRNA or AMPKα1/α2shRNA into the cerebral cortex of immunocompromised mice. AMPK depletion increased survival and reduced tumor growth in all GSC lines (Fig. 3a, b; Supplementary Fig. 2 a–e), while no effect of AMPK-silencing was observed in the GBM serum line U87 (Supplementary Fig. 2f). Control mice (nontarget shRNA) lived for 17–29 days, while mice transplanted with AMPKβ1 shRNA or AMPKα1/α2shRNA-expressing GSCs either lived longer or remained tumor-free (Fig. 3b, c; Supplementary Fig. 2e). Consistent with our in vitro results, expression of a shRNA-resistant cumate-inducible mouse AMPKβ1 completely rescued tumor growth and survival (Fig. 3d–f; Supplementary Fig. 2g, h). AMPK-silenced tumors showed significant residual AMPKβ1 expression and AMPK activity at the tumor and cellular level (Supplementary Fig. 2 i–k) indicating inefficient silencing. The AMPK-silenced tumors were smaller, showed reduced proliferation and increased apoptosis compared to controls (Fig. 3c, g–l). We took a step forward and tested whether repression of AMPK in established tumors enhances survival. Tumors were established using cells expressing both human AMPKβ1 shRNA and cumate-induced mouse AMPKβ1 (that is resistant to human shRNA). Withdrawal of cumate significantly increased survival of tumor-bearing mice (Fig. 3m).

GSC death occurs independent of AMPK-regulated mTOR and autophagy pathways

Cancer cell survival can be positively or negatively regulated by autophagy, depending on the context. AMPK positively regulates autophagy and consequently, AMPK-silenced GSCs showed diminished basal autophagy and autophagy flux as revealed by lower levels of LC3-II and P62 basally and in the presence of the autophagy inhibitor Bafilomycin (Supplementary Fig 3a, b). AMPK-regulated mitophagy has a broad role in mitochondrial homeostasis and could be crucial for survival in some contexts. However, reduced autophagy is unlikely to be the cause of cell death in AMPK-silenced primary GSCs because consistent with others[38, 39], autophagy inhibition alone was insufficient to kill GSCs (Supplementary Fig 3c). AMPK maintains cellular redox state[40, 41] by phosphorylating and inhibiting ACC1, which uses NADPH. In AMPK-silenced cells, hyperactivated ACC1 can deplete NADPH, causing oxidative stress and death that can be rescued by the reducing agent N-Acetylcysteine (NAC)[41]. AMPK silencing indeed raised superoxide anion (Supplementary Fig. 3d), but neither the ACC inhibitor TOFA, nor NAC rescued cell death suggesting that superoxide is not the cause of death of primary GSC lines (Supplementary Fig. 3e). AMPK balances energy expenditure by inhibiting mTORC1, which can drain energy if uninhibited[8, 9]. Indeed, AMPK depletion caused significant drop in ATP (Supplementary Fig. 3f). However, AMPK silencing did not increase mTORC1 activity, and consistent with others[41] the mTORC1 inhibitor rapamycin failed to protect AMPK-silenced GSCs (Supplementary Fig. 3g). AMPK silencing did not significantly affect the expression of stem cell markers in GSCs (Supplementary Fig. 3h). Considering these results, we postulated that

AMPK-depleted GSCs probably die not due to energy drainage but due to a deficit in energy production.

AMPK regulates GSC bioenergetics

To gain molecular insight, we performed *RNAseq*. Analysis of differential gene expression and deregulated pathways showed that bioenergetics of cellular metabolism (glycolysis and mitochondrial function) was the most significantly downregulated pathway in AMPK-depleted GSCs (Fig. 4a). Transcriptional networks controlled by HIF1α, and GABPA/NRF2 - two key transcription factors regulating glycolysis and mitochondria function, respectively[42–47], were downregulated (Fig. 4a; Supplementary Fig. 4a–c), while other pathways (e.g., SREBP-mediated lipid pathway, Notch pathway, aminoglycan biosynthesis, MAP kinase scaffold activity) were upregulated in AMPK-silenced GSCs (Supplementary Fig. 4c). RNA and protein analysis of GSCs and tumors (Fig. 4b–d; Supplementary Fig. 4d, e) confirmed that HIF1α, GABPA and their targets were downregulated in AMPK-depleted cells. Phosphorylation of pyruvate dehydrogenase (PDH) by the HIF1α transcriptional target pyruvate dehydrogenase kinase (PDK) was also reduced (Supplementary Fig. 4e). Despite downregulation of the HIF1α target Glut1, glucose import was not affected (Supplementary Fig. 4f), likely due to compensation by the other glucose transporter Glut3 (Supplementary Fig. 4g).

Functional analysis using two independent AMPKβ1 shRNA confirmed that indeed, both glycolysis and mitochondrial respiration were reduced in AMPK-silenced GSCs (Fig 4e, f) and tumors (Fig 4g, h), but not in long-established GBM serum lines (Fig. 4i, j). Accordingly, energy levels (Fig. 4k), and glucose-induced lactate and citrate production (Fig. 4l, m) and were also reduced. Kinetic flux analysis using ^{13}C glucose showed reduced labeling of several metabolites of glycolysis and TCA cycle in AMPK-depleted cells (Fig. 4n; Supplementary Fig. 5 a–h). Mitochondrial DNA analysis, activity assay and electron microscopy showed reduced mitochondrial mass/number and mitochondrial complex activity in AMPK-silenced GSCs (Fig. 4o–r). Although mechanisms are unclear, in some contexts PGC1α and SIRT1 have been shown to regulate mitochondrial biogenesis and respiration downstream of AMPK[48]. Total and acetylated PGC1α protein (a reaction regulated by the deacetylase SIRT1) remained unchanged in AMPK silenced GSCs (Supplementary Fig. 4h, i). PGC1α overexpression did not rescue mitochondrial defects of AMPK-silenced GSCs (Supplementary Fig. 4j–l). The SIRT1 activator SIRT 1720 partially increased mitochondrial mass and OCR in both WT AMPK-silenced GSCs (Supplementary Fig. 4m, n) perhaps through AMPK-independent mechanisms. Together, our findings indicate the presence of an AMPK regulated transcriptional program important for GBM bioenergetics.

HIF1α transcriptional program is downregulated in AMPK-silenced GSCs

Further molecular analyses showed that both steady-state and hypoxia-induced HIF1α protein levels were reduced in AMPK-silenced cells (Fig. 5a). HIF1α transcript, in the presence of Actinomycin D, was only slightly decreased suggesting that HIF1α transcription and not RNA stability accounts for the decrease in mRNA (Fig. 5b). HIF1α protein also seemed a bit more unstable in AMPK silenced cells (Fig. 5c). Single-cell small molecule

RNA-FISH (sm-FISH)[49] revealed that indeed, HIF1α active transcription was significantly diminished in AMPK-silenced cells (Fig. 5d, e). Accordingly, HIF1α promoter activity and HIF1α DNA-binding to its target genes[32, 33] were also reduced (Fig. 5f, g). Micro-vessel formation, potentially regulated by HIF1α-VEGF or other vasculogenic pathways was also diminished in AMPK silenced tumors (Fig. 5h, i).Consistent with previous reports[32], HIF1α silencing reduced GSC viability (Fig. 5j).

TCA cycle that produces succinate was downregulated in AMPK-silenced cells. Since succinate inhibits prolyl hydroxylases[50] that in turn hydroxylates and destabilizes HIF1α protein[51], we tested if HIF1α is differentially hydroxylated in AMPK silenced cells. More hydroxylated HIF1α was observed in AMPK silenced GSCs, and addition of succinate reduced HIF1α hydroxylation and increased HIF1α stability (Fig. 5k, l). HIF2α plays diverse roles in glioma[32, 52]. We found that HIF2α is overexpressed in AMPK knockdown GSCs, potentially to compensate (although insufficiently) for the loss of HIF1α (Fig. 5k). Finally, inducible overexpression of non-degradable HIF1α partially rescued viability of AMPK-silenced GSCs (Fig. 5m). Together, these results indicate that AMPK plays an important role in regulating HIF1α in GSCs.

GABPA transcriptional program is downregulated in AMPK-silenced GSCs

Consistent with reduced GABPA RNA and protein (Fig 4c, d; Supplementary Fig 4d, e), GABPA binding to its target genes[45, 46] was also diminished in AMPK-silenced cells (Fig. 6a). Transcript levels and target DNA binding of NRF1 (another transcription factor important for mitochondrial function)[45] were upregulated (Fig. 6b, c), likely to compensate (although insufficiently) for the reduction in GABPA. Transcription of genes coordinated by both NRF1 and GABPA (e.g., COX4, mTERF, POLRMT) either did not change or increased slightly (Fig. 6d). GABPA transcribes TFAM, the transcription factor which critically regulates both transcription and replication of the mitochondrial genome[45–47]. Accordingly, silencing of GABPA reduced cell viability and respiration (Fig. 6e–g) and silencing TFAM reduced GSC viability (Fig. 6h, i). Consistent with the role of GABPA in regulating TFAM and mitochondrial function, overexpression of GABPA or TFAM partially rescued viability defects of AMPK-silenced GSCs indicating their function downstream of AMPK (Fig. 6j, k). Since mitochondrial TCA cycle substrates were diminished in AMPK silenced cells, we also tested if their replenishment rescue cell viability. Adding succinate but not pyruvate (since it is already present in the basal medium) partially rescued viability of AMPK-silenced GSCs. The above results indicate that an important mechanism by which AMPK regulates GSC mitochondrial bioenergetics is through GABPA transcription.

AMPK-CREB1 axis regulates HIF1α and GABPA transcription in GSCs

We hypothesized that another transcription factor is a potential molecular link between AMPK and HIF1α / GABPA. Analysis of functional genomics data from ENCODE and Roadmap Epigenomics identified potential CREB1 binding sites in the HIF1α and GABPA promoter/enhancer regions (Supplementary Fig. 6a, b). Indeed, CREB1 chromatin immunoprecipitation (ChIP) showed significant CREB1 enrichment in the GABPA promoter and a potential enhancer distal to HIF1α 3’ region. Importantly, this enrichment was significantly diminished upon AMPK-silencing (Fig. 7a). Accordingly, CREB1 knockdown

reduced HIF1α promoter activity, HIF1α and GABPA transcriptional target expression, cell viability and GSC bioenergetics (Fig. 7b–f). TCGA data analysis showed that CREB1, EP300 (which augments CREB1activity), HIF1α, GABPA and TFAM, as well as phosphorylated CREB1[31] are highly expressed in GBM relative to normal brain (Supplementary Fig. 7a–d). Among these genes although only CREB1 is prognostic in LGG ($p = 0.002$) (Supplementary Fig. 7e), they are important for the biology of human cancer including GBM[31–34, 53]. Thus, these genes are likely highly expressed uniformly across the large majority of GBMs compared to their variable expression in LGG as reported for HIF1α and phosphorylated CREB1[29–31].

Exercise-induced stress activates AMPK to enhance muscle bioenergetics, and active AMPK phosphorylates CREB1 at S133[54–58], a modification that activates CREB1[59]. We tested if this pathway is hijacked during oncogenesis-associated stress in GBM. AMPK silencing by two independent shRNAs reduced (Fig. 7g, h), while pharmacological or physiological AMPK activation enhanced (Fig. 7i) $CREB^{S133}$ phosphorylation in human astrocytes. Accordingly, $pCREB1^{S133}$ staining was also diminished in AMPK β1-silenced tumors (Fig. 7j). To establish a more direct link between CREB phosphorylation, HIF1α and GABPA, we either silenced CREB1 or overexpressed $CREB1^{S133A}$ or $CREB1^{S133E}$ in NHA, and examined levels of HIF1α and GABPA and their downstream glycolysis and mitochondrial targets. Several glycolytic and mitochondrial targets of HIF1α and GABPA were down regulated in $CREB1^{S133A}$ expressing cells and upregulated in $CREB1^{S133E}$ expressing cells (Fig. 7k). Consistent with these results, CREB1 knockdown and $CREB1^{S133A}$ repressed HIF1α and GABPA protein while $CREB1^{S133E}$ increased HIF1α and GABPA (Fig 7l). Accordingly, $CREB1^{S133A}$ expressing tumors clearly showed reduced HIF1α and GABPA protein (Fig 7m).

Acute AMPK activation caused nuclear enrichment of $pCREB1^{S133}$ (Supplementary Fig. 7f, g) in vitro, and in the tumor, nuclear pCREB1 co-localized with pAMPK (Supplementary Fig 7h). Lastly, overexpression of AMPK α, β and γ subunits in normal astrocytes increased CREB1 phosphorylation (Supplementary Fig 7i). However, AMPKβ1 overexpression did not significantly alter proliferation of normal astrocytes (Supplementary Fig 7j). Together, these evidence show a direct link between active AMPK, CREB phosphorylation and HIF1α and GABPA regulated gene expression in GSCs. CREB1 is also phosphorylated at S133 by Protein kinase A (PKA)[59]. However, AMPKβ1 shRNA reduced CREB1 phosphorylation but not that of other PKA substrates indicating its specificity for CREB1. Importantly, the PKA activator forskolin phosphorylated PKA substrates in both NT shRNA and AMPKβ1 shRNA cells but only CREB1 in NT shRNA cells (Supplementary Fig. 7k). The failure of forskolin to phosphorylate CREB1 in AMPKβ1 shRNA cells showed that AMPK plays a specific and dominant role in CREB1 phosphorylation in GBM.

To test if $Creb1^{S133}$ phosphorylation plays a critical role in GBM pathogenesis, we expressed inactive inducible phospho-mutant $CREB1^{S133A}$ or phosphomimetic $CREB1^{S133E}$ and examined GSC viability. $CREB1^{S133A}$ reduced ATP levels and diminished viability (Fig. 8a, b), while $CREB1^{S133E}$ rescued viability defects of AMPKβ1-silenced cells (Fig. 8c). When transplanted in the brain, inducible expression of $CREB1^{S133A}$ significantly

delayed tumorigenesis and improved survival in mice (Fig. 8d, e) indicating the significance of CREB1^{S133} phosphorylation in GBM.

Systemic deletion of AMPK is tolerated in adult mice

We found that various types of cancer-associated stress chronically activate AMPK and that GSCs hijack a stress response pathway conserved in normal cells, using it to survive. This suggests that AMPK is an appropriate target in GBM, and if so, the effect of deleting AMPK in GBM mouse models and the effects of whole-body AMPK inhibition to check systemic tolerance warrant investigation. We did not use Compound C, the only reagent, sometimes used as an AMPK inhibitor because of its nonspecificity. Remarkably, adult mice with systemic AMPK knockout did not show overt metabolic phenotype and lived a normal life span (Supplementary Fig. 8) underscoring the potential utility of AMPK inhibitors in the treatment of GBM and perhaps other human cancers where AMPK is activated.

DISCUSSIOIN

In this study, we show that oncogenesis-associated stress chronically activates the cellular energy sensor AMPK in GBM. Our results are consistent with the high expression of active AMPK in glioma and its requirement in proliferation of oncogenic mouse astroglia[11, 12, 60]. Why the established GBM serum lines remained viable and formed tumor independent of AMPK is unclear. Decades of culture could have altered genetic, epigenetic and metabolic landscape of these lines[61] that have become adapted and evolved AMPK-independent growth and survival pathways. AMPK was also found to enhance glioma cell viability by inducing lipid import *in vitro*[62]. While this remains a possibility *in vivo*, our primary GSC lines are grown in serum-free media containing only two essential fatty acids precluding their dependence on serum-derived non-essential fatty acids *in vitro*. In contrast to our results, the metabolic stressor AICAR that activates AMPK, inhibited growth of an established glioma serum line U87MG[16]. While we could not directly compare their results with ours, we and others have shown that AICAR suppresses cancer including glioma through multiple AMPK-independent mechanisms[12]. Previous pharmacological approaches are not fully reconcilable with later genetic studies, and there is more recent appreciation that AMPK can play a context-dependent function in cancer[3]. Consistent with tissue and species-specific effects of AMPK, AMPKα1 suppressed lymphomagenesis in a Myc mouse model[10], while active AMPK was required for tumor growth in other models[17–22, 41, 63]. Interestingly, in a functional metabolic screen, AMPKβ1 was identified as a critical prostate cancer cell survival gene[37], which together with our studies underscore a particularly important function of the AMPKβ1-containing complex in cancer cell survival and tumor growth.

While the role of AMPK in cancer is complex[3], several mechanisms are known by which it checks cellular growth and proliferation[8, 9, 64, 65]. In contrast, very few mechanisms are known by which it promotes survival and growth in other contexts. Through comprehensive genetic analysis, we here show a mechanism by which AMPK supports tumor bioenergetics, growth and survival in human glioblastoma. We show that by phosphorylating CREB1, which occurs abundantly in GBM[31], AMPK enhances HIF1α and GABPA transcription to

support GBM bioenergetics (Fig. 8f). HIF1α can attenuate mitochondrial respiration through its transcriptional target PDK that phosphorylates and inhibits PDH[66]. Therefore, HIF1α downregulation and reduced PDH phosphorylation was expected to augment mitochondrial respiration in AMPK-silenced cells. Perhaps, downregulation of GABPA-TFAM, that are critical to mitochondrial transcription and replication overrides the stimulatory effect of hypophosphorylated (active) PDH and diminishes mitochondrial function in AMPK-silenced GSCs.

The evidence that AMPK phosphorylates CREB at S133 (also a PKA site) *in vitro* and *in vivo* is strong[54–58]. AMPK also strongly phosphorylated a chimeric peptide of CREB1 and ACC (a bonafide AMPK substrate) that lacked the AMPK phosphorylation site in ACC (Ser78), indicating specificity of AMPK for CREB1. In fact, the *Vmax* of AMPK for the CREB1 peptide is comparable to that for the ACC peptide (12.3 pmol/min versus 9.3 pmol/min)[58]. High levels of nuclear CREB1 is expressed in GBM[31]. We speculate that the AMPKβ1 complex, which is enriched in the nucleus[67] phosphorylates CREB1 and potentially other nuclear targets[20]. It remains to be seen what specific role AMPK or the CREB1 transcriptional program (that can be regulated independent of AMPK) plays during the step-wise evolution of human cancer.

METHODS

Reagents

The following reagents were used : Oligomycin, FCCP, Antimycin, Rotenone, Tunicamycin, Thapsigargin, Camptothecin B, Hydroxyurea, Puromycin, Doxycycline, DAPI, Hydrogen peroxide, Formamide, STO-609, KU55933, NAC, TOFA, PKI, Forskolin, Methyl Pyruvate, Sodium Succinate, Cycloheximide and Chloroquine, Glucose, Resveratrol and DMSO (all from Sigma), G418 (Invitrogen), Compound 991 (a gift from David Carling), A769662 and Rapamycin (LC Laboratories) and SIRT1720 (Apen Biotechnology). The VectaStain ABC kit was from Vector Laboratories. D-Luciferin was from Perkin Elmer. Compound C was from EMD Millipore. Isolectin B4 (IB4; cat# DL-1207) (Vector Laboratories, kind gift from Elisa Boscolo).

Cell Culture

Human primary glioblastoma lines were established from freshly resected tumors either in our laboratory under a University of Cincinnati institutional review board (IRB) approved protocol, or obtained from our collaborators (University of Alabama). Informed consent was taken from all subjects. Cells were maintained as suspension cultures in UltraLow attachment plates in glioma stem cell (GSC) medium that contained glucose-free DMEM-F/12 supplemented with 5mM glucose, B27, EGF (10 ng/ml), bFGF (10 ng/mL), GlutaMAX, and heparin (5 mg/mL). Adherent glioma serum lines (U87, T98G, and A172) and HEK 293T cells were purchased from ATCC and were not re-authenticated. The U87 line was recently identified as another GBM line. We completed our experiments long before this misidentification was published. These lines were maintained in glucose-free DMEM supplemented with 5mM glucose and 10% FCS and were used in our earlier publication. Normal human astrocytes (NHA) were purchased from Lonza Group Ltd. and

immortalized with retroviral expression of Large T-antigen (pBabe-puro TcDNA, #14088, Addgene). NHA was maintained in glucose-free DMEM supplemented with 5mM glucose and 10% FCS. Culture conditions of NHA did not influence the effect of AMPK shRNA. We switched NHA culture medium temporarily to GSC medium and tested the effect of AMPK shRNA and the results remained consistent to what we observed in FCS-containing medium. All lines were routinely checked for mycoplasma every other week using mycoplasma-specific PCR. Primary GSC lines and NHA were analyzed by STR analysis. For proliferation and viability analysis, both direct counting using Trypan blue method and a fluorescence-based method (CellTiter-Fluor; Promega) were used.

Western Blotting

Western blot (WB) analysis was carried out following standard methods as before[12]. Each experiment was successfully carried out for two to three times. Antiboides were validated by using positive and negative control tissues and cells. Antibody information is provided in Supplementary Table 1.

Immunohistochemistry (IHC)

Fresh frozen human tissues and paraffin sections were obtained from the tissue repository at The University of Cincinnati under a UC IRB approved protocol. Mouse high grade glioma tissue were obtained from a transgenic glioma mouse model[35]. IHC was done as previously described[12]. Mice were anesthetized, perfused intracardially with 4% PBS, tumors were dissected out and processed for paraffin embedding and sectioning. Antibody validation was done using multiple positive and negative control tissues and cells. Antibody information is provided in Supplementary Table 1.

Hypoxia

After 72h of shRNA infection, cells were maintained at hypoxia in a controlled atmosphere chamber (Don Whitley Scientific) with a gas mixture containing 0.5% to 1% O2, 5% (vol/vol) CO2, and 94% (vol/vol) N2 at 37 °C for the indicated time depending on the experiment. Cells were harvested for downstream processing inside the chamber.

Glucose import

A glucose uptake assay was performed using 100 μM 2-[N-(7-nitrobenz-2-oxa-1,3-diazol-4-yl)amino]-2-deoxy-D-glucose (2-NBDG; Invitrogen), followed by FACS detection (BD Bioscience). After 72 h of shRNA infection, 10^5 cells/mL were incubated with 2-NBDG () for indicated time points anddata from 10,000 single-cell events were collected. Original FACS plots are provided in Supplementary Source File.

Quantification of Superoxide anion

The intracellular levels of Superoxide (O_2^-) were measured with MitoSOX™ Red (Invitrogen). 1×10^5 cells were plated in a 12-well plate, treated with MitoSOX Red (5 micromolar) for 10 min at 37 °C, washed with PBS and analyzed in FACScan flow cytometers. Original FACS plots are provided in Supplementary Source File.

Lentivirus Preparation and Production of Stable shRNA-Expressing Cell Lines

Several independent shRNA sequences were screened for each of the used human target genes, and the sequences which exhibited maximal knockdown were used for the study. Most shRNA clones (in pLKO.1 plasmid) were from the Sigma Mission RNAi shRNA library. The AMPK β2 shRNA clone was purchased from OriGene. pLKO.1-puro scrambled (NT) shRNA (Sigma) was used as a negative control. ShRNAs were prepared in 293T cells as before[12]. Overexpression clones in pInducer 20 were selected with G418 (700 microgram/mL). Efficacy of knockdown/overexpression was assayed by WB or Q-RTPCR. The sequences that exhibited maximal knockdown/overexpression were used for the study. ShRNA sequences are provided in Supplementary table 2.

Crispr/Cas9 gene knockout

CRISPR/Cas9 – allows for specific genome disruption and replacement in a flexible and simple system resulting in high specificity and low cell toxicity. 3 guide RNAs (gRNAs) were designed to knockout target sequence of the AMPK β1 locus. Donor and gRNAs were purchased from Blue Heron Biotech, WA, USA). The f target sequences cloned into pCas-Guide vector are provided in Supplementary table 2. The efficiency of the CRISPR/Cas9 was assessed by immunoblot assay.

Mass spectrometry of metabolites

Profiling of glycolysis, TCA cycle, and nucleotide metabolites was carried out by solvent extraction followed by liquid chromatography-mass spectrometry. Cells were treated with 5 mM D-Glucose (^{U13}C6, CLM-1396, from Cambridge Isotope) for different time points up to 90 minutes. Metabolites were detected using LC- tandem-quadrupole mass spectrometry. The investigators were blinded to allocation during experiments and outcome assessment.

Bioenergetics experiments

ATP quantification in GSCs (1×10^5 cells) was done using the ApoSENSOR ATP Luminescence Assay Kit (BioVision). ECAR and OCR were analyzed using the XF^{e}96-Analyzer (Seahorse Biosciences) as before[12]. GSCs were attached to the wells with Cell Tak (Corning). Tumor tissues from flank xenografts were surgically harvested and one millimeter uniformly thick sections were incised using metal tissue matrices. From these brain sections, 2 mm diameter circular pieces were cut out using biopsy punches (Miltex, York, PA). Tissues of equal weight were analyzed in the Seahorse analyzer as described[67]. Extracellular lactate and citrate were measured from culture supernatants using lactate and citrate assay kits (Biovision, Milpitas, CA).

Plasmids and Clonings

Mouse β1 and β2 ORFs were purchased from Origene and subcloned into lentiviral vectors CMVTV and FCIV, respectively. Dominant negative AMPKa2 (a gift from Russell Jones) was cloned into FCIV lentiviral vector[67]. PLenti-PGK-KRAS4A (G12V) cat#35634 was from Addgene and pLV EGFRvIII Hygro was gifted by Dr. Frank Furnari. For overexpression studies, genes were subcloned into the doxycycline-inducible lentiviral vector pInducer 20. Human AMPK β1 was also subcloned into cumate-inducible SparQ all-

in-one lentivirus (gift from System Biosciences, Paolo Alto, CA). Human HIF1α (Acc# KR710294.1), GABPA (Acc# BC035031.2) and TFAM (Acc# BC126366.1) were PCR amplified to add attB sites using TFAM, GABPA and HIF1α primers. Primer sequences are provided in Supplementary table 3.

The PCR fragments were gel purified and transferred into pDONR221 and pInducer20 using Gateway recombination as above. Sequences of all clones were confirmed by Sanger sequencing at the CCHMC DNA Core.

To generate mCreb1 S133A, mutagenesis was performed on mCreb1 (Acc # BC021649) in pCMV-SPORT6 with the Phusion Site Directed Mutagenesis Kit (Thermo Scientific, catalogue #F-541). The open reading frame of wt mCreb1 and mCreb1 S133A was PCR amplified to add attB recombination sites using Herculase II Fusion DNA Polymerase (Agilent Technologies, catalogue #600675-51).

The PCR fragments were gel purified using the QIAquick Gel Extraction Kit (QIAGEN, cat # 28704) and transferred by BP recombination reaction into pDONR221 (Invitrogen, cat # 12536-017) using Gateway BP Clonase II Enzyme Mix (Life Technologies, catalogue #11789-020) and subsequently by LR recombination reaction into pInducer20 using Gateway LR Clonase II Enzyme Mix (Life Technologies, catalogue #11791-020). To generate mCreb1 S133E, mutagenesis was performed directly on mCreb1 in pInducer20 using the Phusion Site Directed Mutagenesis Kit and primers 5'-AAGGAGGCCTGAGTACAGGAAAATTT-' and 5' -GAAAGGATTTCCCTTCGTTTTTGG-3'

For cloning into cumate-inducible SparQ vector, mouse AMPKβ1 cDNA was amplified from pcMV-Sport6 mouse AMPK beta1. Restriction sites were added by PCR using the following primers: forward 5′- GCTAGCATGGGCAACACGAGC -3′ and reverse 5′-GCGGCCGCTCATCATATCGGCTTGTAGAGGAGGGT -3′. The PCR product and the recipient plasmid SparQ All-in-one Cumate Switch Vectors (System Biosciences Cat# QM812B-1) were digested with NheI and NotI. The ligation reaction was transformed into GC10 Competent Cells (Sigma), and plasmid DNA was purified with QIAGEN Hi Speed Plasmid Midi Kit (Qiagen).

Sirt3 Flag (Plasmid # 13814) and pcDNA4 myc PGC-1 alpha (Plasmid # 10974) were purchased from Addgene.

HIF1α Promoter activity assay

Cells were seeded onto 6-well plates, co-transfected with the HRE luciferase reporter and control pSV40-Renilla (gifts from Dr. Gang Huang) for 24h. Transfection medium was washed off and cells were further incubated for 24h. Cell extracts were analyzed using the Dual-Luciferase Assay System (Promega).

Quantification of mitochondrial mass

Cells were treated with shRNA expressing viral particles and after 72h, genomic DNA was prepared using QIAamp DNA kit (Qiagen). mtDNA and genomic DNA were detected using

ND4 and β-actin primers, respectively. PCR was used to compare fold change in total mitochondrial content.

RNA extraction and qRT-PCR

2 micrograms of total RNA (RNeasy kit, Qiagen) was utilized for first strand cDNA synthesis with oligo-dT primers and Superscript II Reverse Transcriptase (Invitrogen). qRT-PCR was performed using SYBR® Green PCR Master Mix (Applied Biosystems) and Quantitect primers (Qiagen) in an ABI PRISM 7900 Sequence Detection System (Applied Biosystems). Relative mRNA expression was calculated using the comparative Ct method after normalization to a loading control. Samples were run in triplicates with a primer-limited probe for the reference gene (Actin or HPRT). Primers are provided in Supplementary table 3.

Orthotopic Xenograft

All animal procedures were carried out in accordance with the Institutional Animal Care and Use Committee (IACUC)-approved protocol of Cincinnati Children's Hospital Medical Center (CCHMC; Cincinnati, OH). The study is compliant with all relevant ethical regulations regarding animal research. Animals were monitored daily by animal care personnel. For orthotopic implantation, 1 X 10^4 primary human GBM cells were stereotactically injected into the left striatum of NOD-SCID IL2Rg^{null} mice. Both male and female mice were used. Randomization of mice for this study was not necessary. For *in vivo* bioluminescent imaging, luciferase expressing cells were established by infection with plenti-CMV-luc viral particles (a gift from Dr. Susanne Wells) and tumor growth was monitored using IVIS 200 system. Five minutes before bioluminescence imaging, mice were anesthetized and injected (intraperitoneally) with luciferin (150 mg/kg) and imaged using IVIS (Xenogen). All mice were euthanized following observation of lethargy and/or neurologic symptoms. For flank xenografts, 2X10^6 cells were injected subcutaneously and imaged using IVIS. These tumors were harvested for ex-vivo bioenergetics experiments. In mice which required cumate injections, animals were injected with cumate (150mg/Kg) from day of orthotopic cell implantation every alternate day until animals were euthanized. The investigators were not blinded to allocation during experiments and outcome assessment.

Culture of human tumor cells from Orthotopic Xenografts

Tumor cells were isolated from NT shRNA or AMPKβ1 shRNA tumors and passaged once. Purity of human cells were determined by PCR with human and mouse-specific DNAPolE and Intracisternal A-particle primers, respectively (not shown). Determination of lentiviral copy number was determined by PCR showed a lower AMPKβ1 shRNA lentiviral integration compared to NT shRNA (3.15 ± 0.62 copies of NT versus *1.33 ± 0.31 copies* of beta1 shRNA).

Generation of whole-body AMPK knockout mice

AMPK alpha1−/−, Alpha2 lox/lox mice (BL/6; kind gifts from Benoit Viollet) and Rosa26 –CreER (BL/6; kind gift from Dr. Ashish Kumar; originally from NCI), were crossed.

AMPKβ1lox/lox mice obtained Sanger Center and AMPK beta2−/− mice that were generated in our lab (and crossed for >10 generations with BL/6 mice) were also crossed with Rosa26–CreER mice. Mice were injected with Tamoxifen (225 microgram/gram body weight; i.p.) at six months of age, every day for three consecutive days. After one week, tissues were harvested (n=2 mice/genotype). Recombination efficiency was determined by Western blot using AMPKα and AMPKβ antibodies. Body weight was recorded once a month and death records were used to generate survival plot. Randomization of mice for this study was not done. Genotyping primers are provided in Supplementary Table 3:

Electron microscopy

Cell pellets were fixed in 3% Glutaraldehyde/0.2M Sodium Cacodylate buffer pH7.4 for at least 1 hour at 4°C. After fixation, the samples were washed 3X with Cacodylate buffer and post-fixed with 1% Osmium tetroxide/.2M Sodium Cacodylate buffer pH 7.4. After post-fixation, cells were washed 2X with Cacodylate buffer, followed by 1X with ddH20. Samples were gently resuspended in 1.5% Agarose (type IX ultra-low gelling) and centrifuged at 1000g for 5 min and processed as before[68]. All images were taken using a 120-kV transmission electron microscope (Hitachi, H-7650, V01.07, Tokyo, Japan)

Immunofluorescence microscopy

Tissue processing for frozen sections was done as before[67, 68]. Fluorescent images were taken on a Nikon AZ-100 multizoom microscope equipped with a Nikon DS-Ri1 camera. Confocal images were taken in Nikon C2 confocal microscope. pACC and IBA1 were both rabbit antibodies and therefore a tyramide based signal amplification was utilized (tyramide amplification kit; Thermo Fisher #T20932). Antibody information is provided in Supplementary Table 1.

Mitochondrial Complex activity

Cells were sonicated in 0.5 ml ice-cold 5 mM KH_2PO_4 (pH 7.5), 1% Digitonin, and then used for electron transport chain (ETC) enzyme assays. ETC enzymes were assayed at 30° C using a temperature-controlled spectrophotometer Shimadzu UV-1600. Activity of complex I (NADH:CoQ reductase) was measured in 5 mM KH_2PO4 (pH 7.5), 5 mM $MgCl_2$, 0.24 mM CoQ1, 0.5 mM KCN, 1 mg/ml BSA, and 2.4 μg/ml Antimycin A. Reaction was initiated with 0.02 mM NADH and reduction of absorbance at 340 nm was recorded with spectrophotometer before and after addition of rotenone (final concentration 2 μg/ml). Activity of complex I+III (NADH:cytochrome *c* reductase) was measured in 5 mM KH_2PO_4 (pH 7.5), 5 mM $MgCl_2$, 0.24 mM CoQ1, 0.5 mM KCN, 1 mg/ml BSA, 0.12 mM cytochrome *c* (oxidized form). Reaction was initiated with 0.02 mM NADH and increase of absorbance at 550 nm was recorded with spectrophotometer before and after addition of Antimycin A (final concentration 2 μg/ml). Activity of complex IV (cytochrome *c* oxidase) was measured in 50 mM KH_2PO_4 (pH 7.5), 2 μg/ml rotenone, and 0.03 mM reduced cytochrome *c* at 550 nm. Activity of complex V was measured in 50 mM Tris (pH 8.0), 5 mg/ml BSA, 20 mM $MgCl_2$, 50 mM KCl, 15 μM FCCP, 5 μM Antimycin A, 10 mM phosphoenol pyruvate, 2.5 mM ATP, 2 U/ml of lactate dehydrogenase and pyruvate kinase, and 0.02 mM NADH. Reaction was initiated by adding cell lysate followed by reduction of absorbance at 340 nm before and after addition of 2 μM of Oligomycin. Citrate synthase

(CS) assay media contained 0.1 mM 5,5′-dithiobis (2-nitrobenzoic acid); 3-carboxy- 4-nitrophenyl disulfide (DTNB), 0.25% Triton X-100, 0.5mM oxaloacetate, 0.31 mM acetyl CoA, 50 mM Tris-HCl, pH 8.0. CS activity was calculated by increasing absorbance at 412 nm using extinction coefficient for TNB 13.6 $mM^{-1} \times cm^{-1}$.

RNAseq

1 microgram of total RNA from NT or AMPKβ1 shRNA expressing GSCs was prepared three days after lentivirus transduction and was used for mRNA library preparation. Completed libraries were sequenced on an Illumina HiSeq2000 in Rapid Mode, generating 20 million or more high quality 50 base long single end reads per sample. RNA-Seq analysis was based on the TopHat/Cufflinks pipeline. Data was processed through NetWalker[2], an application platform that allows interactive comparative analysis of most active networks and functional processes. The reference annotation used was based on the UCSC knownGenes table. This method allows accurate quantification of expression of all transcripts, known or novel. BAM files have been deposited to GEO (Accession # GSE82183). The investigators were blinded to allocation during experiments and outcome assessment.

Computational identification of putative CREB1 binding sites

Analysis of functional genomics data from ENCODE and Roadmap Epigenomics identified potential CREB1 binding sites in the HIF1α and GABPA promoter regions. Since no ChIP-seq datasets exist describing CREB1 binding in cell types relevant to this study, we devised a computational method for identifying likely CREB1 binding sites in relevant cell types proximal to HIF1α and GABPA. We first compiled datasets indicative of likely regulatory regions from ENCODE and Roadmap Epigenomics, including DNase-seq, ChIP-seq for specific transcription factors, and models combining specific histone marks into likely regulatory states[3]. We restricted our analysis to experiments performed in cell types relevant to this study: glial cell lines (U87, NH-A), glioblastoma cell lines (D54, M059J), neuronal (PFSK-1, T98G) cell lines, neuronal stem cells, and cortex and ganglion eminence-derived neurospheres. We identified likely regulatory regions located within 100kb of either gene by taking the union of the genomic coordinates covered by these datasets. Next, for each of these putative “relevant” regulatory regions, we restricted our attention to regions containing ChIP-seq peaks for CREB1 in any cell type. The resulting regions are therefore first bound by CREB1 in at least one experiment, and second, likely regulatory regions in relevant cell types. Using this approach, we identified three regions putatively bound by CREB1 one in the promoter of GABPA and two, in HIF1α regulatory regions. We designed primers to capture the center of each CREB1 ChIP peak.

Chromatin Immunoprecipitation assays (ChIP)

ChIP assays were performed using 500 micrograms of chromatin. Chromatin was sonicated to fragments of ~500 bp and immunoprecipitated using 1 microgram of ChIP-grade antibodies: HIF1α (NB100–134, Novus Biological), GABPA (sc-22810X, Santa Cruz Biotechnology), CREB1 (9104, Cell Signaling Technology) and with irrelevant IgG antibodies of mouse and rabbit origin and recovered using protein A/G magnetic beads (from Magna ChIP™ A/G, Millipore). The precipitated DNA was amplified by real-time

qPCR, using primer sets designed to amplify regions of the target genes. ChIP primer sequences are provided in Supplementary Table 3:

Single Molecule RNA FISH

Control or AMPK β1shRNA expressing GSC10 cells were grown on #1.5 cover glass and fixed with 3.7% formaldehyde in 1X PBS for 10 minutes at room temperature. Fixed cells were washed twice with 1X PBS, permeabilized with 70% EtOH for 2 hours at 4°C, then treated with wash buffer (2x SSC, 10% formamide) for 5 minutes at room temperature. Fixed, permeabilized cells were then hybridized to Stellaris sm FISH probes against human HIF1α conjugated with Quasar 570 dye in hybridization buffer (100 mg/mL dextran sulfate and 10% formamide in 2X SSC) overnight at 37°C. Hybridized cells were washed in wash buffer 30 minutes at 37°C, treated with DAPI, and mounted with Vectashield. Cells were imaged on a Nikon A1 laser scanning confocal microscope equipped with GaAsP detectors using 561nm excitation for Quasar 570 dye and 405nm excitation for DAPI. A 100X NA 1.45 objective was used for imaging and cells were sampled at Nyquist resolution (0.12um pixel size). Z-stacks of ~5micrometer were acquired to capture the entire cell. Total number of transcripts per cell was quantified using Bitplane Imaris. Cells were analyzed using "Spots" algorithm with a spot size of the diffraction limit (0.280um).

Statistics and Reproducibility

For all *in vitro* and *ex vivo* experiments three to ten technical replicates were used. Each experiment was repeated successfully two to three times as indicated in figure legend. For *in vivo* mouse orthotopic xenograft studies, 4–8 mice per genotype were used, and for body weight and survival analysis of wildtype and AMPK KO mice, 12 mice per genotype were used experiments. Sample size was chosen with consideration to ensure adequate statistical power to detect prespecified effects. GraphPad Prism software was used to generate and analyze survival plot, and R was used to generate box plots from TCGA data. *P* values were generated using a two-sided *t*-test to calculate statistical significance with $P < 0.05$ representing a statistically significant difference. No statistical method was used to predetermine sample size. Kaplan–Meier analysis with log-rank posthoc test was used for survival studies. There was no need to exclude mice from analysis except the few that died during surgical transplantation of tumor cells. The number of indicated mice represents the total number of mice used and processed for each experiment. Because investigators were aware of the cell genotypes which they themselves transplanted in mice, there was no option for them to remain blinded to allocation for the *in vivo* experiments. The investigators were blinded to allocation for IHC analyses. For orthotopic xenograft studies, mice were euthanized at the ethical endpoint when they failed to meet the predetermined CCHMC IACUC quality-of-life guidelines. No mice that completed in vivo studies were excluded from analyses. There are no limitations in reproducibility for experiments.

Data Availability

Statistical source data is available in Supplementary Table 4. RNA-Seq BAM files have been deposited to GEO (Accession # GSE82183).All other supporting data of this study are available from the corresponding author on reasonable request.

Supplementary Material

Refer to Web version on PubMed Central for supplementary material.

Acknowledgments

We thank Sunghak Kim for maintaining and providing primary GSC lines, Ashwini Hinge for help with flow cytometry, Gang Huang for providing HRE luciferase reporter construct and help with ChIP experiments, James Bridges for providing constitutive active HIF1α, Susanne Wells for plenti-CMV-luc plasmid, Steve Elledge for providing pInducer plasmid, Russell Jones for AMPKα2 dominant negative plasmid, Frank Furnari for pLV EGFRvIII Hygro plasmid, Paul Mischel for U87EGFRvIII glioma cells, David Carling for providing Compound 991, Xiaona Liu for assistance with experiments, Punam Malik for providing assistance in determining lentiviral copy number, Elisa Boscolo for providing Isolectin B4, Benoit Viollet for providing AMPK alpha1−/− and AMPK alpha2 lox/lox mice and Ashish Kumar for providing Rosa26 CreER mice (originally from NCI). This work was supported by the CCTST1 Translational Grant Award; Pilot Innovation award, CCHMC; University of Cincinnati Cancer Center Affinity Grant Award, CancerFreeKids and National Institute of Health (1R01NS075291-01A1 and 1R01NS099161-01) (all to B.D).

AUTHOR CONTRIBUTIONS

B.D. and R.C conceived the experiments, analyzed data and wrote the manuscript. R.C. performed most of the experiments. Q.F., J.A. R.M, and J.A. performed additional experiments. G.C. helped with electron microscopy. N.R, R.W. and L.M.C provided valuable reagents and experimental suggestions. N.R. also helped in manuscript editing. Y.H. performed and Z.K. supervised mitochondrial complex activity measurements. M.K. helped with smFISH experiments. M.W. and X. C. provided bioinformatic support for transcription factor analysis. A.K. helped identification of GBM patient samples. C.M. performed surgery and helped coordinate tissue procurement from the OR, I.N. provided several primary GSC lines. N.D. and K.K provided bioinformatic support for RNAseq and TCGA data analysis. N.D. also performed statistical analysis.

References

1. Hardie DG. AMP-activated protein kinase: maintaining energy homeostasis at the cellular and whole-body levels. Annual review of nutrition. 2014; 34:31–55.
2. Carling D, Thornton C, Woods A, Sanders MJ. AMP-activated protein kinase: new regulation, new roles? The Biochemical journal. 2012; 445:11–27. [PubMed: 22702974]
3. Dasgupta B, Chhipa RR. Evolving Lessons on the Complex Role of AMPK in Normal Physiology and Cancer. Trends in pharmacological sciences. 2016; 37:192–206. [PubMed: 26711141]
4. Iseli TJ, et al. AMP-activated protein kinase beta subunit tethers alpha and gamma subunits via its C-terminal sequence (186–270). The Journal of biological chemistry. 2005; 280:13395–13400. [PubMed: 15695819]
5. Shaw RJ, et al. The tumor suppressor LKB1 kinase directly activates AMP-activated kinase and regulates apoptosis in response to energy stress. Proceedings of the National Academy of Sciences of the United States of America. 2004; 101:3329–3335. [PubMed: 14985505]
6. Hawley SA, et al. Calmodulin-dependent protein kinase kinase-beta is an alternative upstream kinase for AMP-activated protein kinase. Cell metabolism. 2005; 2:9–19. [PubMed: 16054095]
7. Carling D, Zammit VA, Hardie DG. A common bicyclic protein kinase cascade inactivates the regulatory enzymes of fatty acid and cholesterol biosynthesis. FEBS letters. 1987; 223:217–222. [PubMed: 2889619]
8. Inoki K, Zhu T, Guan KL. TSC2 mediates cellular energy response to control cell growth and survival. Cell. 2003; 115:577–590. [PubMed: 14651849]

9. Gwinn DM, et al. AMPK phosphorylation of raptor mediates a metabolic checkpoint. Molecular cell. 2008; 30:214–226. [PubMed: 18439900]
10. Faubert B, et al. AMPK is a negative regulator of the Warburg effect and suppresses tumor growth in vivo. Cell metabolism. 2013; 17:113–124. [PubMed: 23274086]
11. Rios M, Foretz M, Viollet B, et al. AMPK activation by oncogenesis is required to maintain cancer cell proliferation in astrocytic tumors. Cancer research. 2013; 73:2628–2638. [PubMed: 23370326]
12. Liu X, et al. Discrete mechanisms of mTOR and cell cycle regulation by AMPK agonists independent of AMPK. Proc. Natl. Acad. Sci. USA. 2014; 111:E435–44. [PubMed: 24474794]
13. Swinnen JV, et al. Mimicry of a cellular low energy status blocks tumor cell anabolism and suppresses the malignant phenotype. Can.Res. 2005; 65:2441–2448.
14. Tang YC, Williams BR, Siegel JJ, Amon A. Identification of aneuploidy-selective antiproliferation compounds. Cell. 2011; 144:499–512. [PubMed: 21315436]
15. Dowling RJ, Zakikhani M, Fantus IG, Pollak M, Sonenberg N. Metformin inhibits mammalian target of rapamycin-dependent translation initiation in breast cancer cells. Can.Res. 2007; 67:10804–10812.
16. Guo D, et al. The AMPK agonist AICAR inhibits the growth of EGFRvIII-expressing glioblastomas by inhibiting lipogenesis. Proc. Natl. Acad. Sci. USA. 2009; 106:12931–7.
17. Yan M, et al. The tumor suppressor folliculin regulates AMPK-dependent metabolic transformation. J. Clin. Invest. 2014; 124:2640–2650. [PubMed: 24762438]
18. Laderoute KR, et al. 5′-AMP-activated protein kinase (AMPK) supports the growth of aggressive experimental human breast cancer tumors. J. Biol. Chem. 2014; 289:22850–22864. [PubMed: 24993821]
19. D'Amico D, et al. Non-canonical Hedgehog/AMPK-Mediated Control of Polyamine Metabolism Supports Neuronal and Medulloblastoma Cell Growth. Dev.Cell. 2015; 35:21–35. [PubMed: 26460945]
20. Bungard D, et al. Signaling kinase AMPK activates stress-promoted transcription via histone H2B phosphorylation. Science. 2010; 329:1201–5. [PubMed: 20647423]
21. Laderoute KR, et al. 5′-AMP-activated protein kinase (AMPK) is induced by low-oxygen and glucose deprivation conditions found in solid-tumor microenvironments. Mol. Cell. Biol. 2006; 26:5336–5347. [PubMed: 16809770]
22. Liu L, et al. Deregulated MYC expression induces dependence upon AMPK-related kinase 5. Nature. 2012; 483:608–612. [PubMed: 22460906]
23. Shackelford DB, et al. mTOR and HIF-1alpha-mediated tumor metabolism in an LKB1 mouse model of Peutz-Jeghers syndrome. Proc Natl Acad Sci U S A. 2009; 106:11137–42. [PubMed: 19541609]
24. Kishton RJ, et al. AMPK Is Essential to Balance Glycolysis and Mitochondrial Metabolism to Control T-ALL Cell Stress and Survival. Cell Metab. 2016; 23:649–62. [PubMed: 27076078]
25. Wu S, et al. AMPK-mediated increase of glycolysis as an adaptive response to oxidative stress in human cells: implication of the cell survival in mitochondrial diseases. Biochem. Biophys. Acta. 2012; 1822:233–47. [PubMed: 22001850]
26. DoménechE E, et al. AMPK and PFKFB3 mediate glycolysis and survival in response to mitophagy during mitotic arrest. Nat Cell Biol. 2015; 17:1304–16. [PubMed: 26322680]
27. Almeida A, et al. Nitric oxide switches on glycolysis through the AMP protein kinase and 6-phosphofructo-2-kinase pathway. Nat Cell Biol. 2004; 6:45–51. [PubMed: 14688792]
28. Fumarola C, et al. Effects of sorafenib on energy metabolism in breast cancer cells: role of AMPK-mTORC1 signaling. Breast Cancer Res Treat. 2013; 141:67–78. [PubMed: 23963659]
29. Reszec J, et al. The expression of hypoxia-inducible factor-1 in primary brain tumors. Int J Neurosci. Sep; 2013 123(9):657–62. [PubMed: 23550771]
30. Mayer A, et al. Differential expression of HIF-1 in glioblastoma multiforme and anaplastic astrocytoma. Int J Oncol. Oct; 2012 41(4):1260–70. [PubMed: 22825389]

31. Barresi V, et al. p-CREB expression in human gliomas: potential use in the differential diagnosis between astrocytoma and oligodendroglioma. Human pathology. 2015; 46:231–238. [PubMed: 25476123]
32. Li Z, et al. Hypoxia-inducible factors regulate tumoregenic capacity of glioma stem cells. Cancer Cell. 2009; 15:501–13. [PubMed: 19477429]
33. Fan Y, et al. Profilin-1 phosphorylation directs angiocrine expression and glioblastoma progression through HIF1a accumulation. Nat. Cell Biol. 2014; 16:445–56. [PubMed: 24747440]
34. Rodel L, et al. Active CREB1 promotes a malignant TGFbeta2 autocrine loop in glioblastoma. Cancer Discov. 2014; 10:1230–41.
35. Chow LM, et al. Cooperativity within and among Pten, p53, and Rb pathways induces high-grade astrocytoma in adult brain. Cancer cell. 2011; 19:305–316. [PubMed: 21397855]
36. Chae YC, et al. Control of tumor bioenergetics and survival stress signaling by mitochondrial HSP90s. Cancer cell. 2012; 22:331–344. [PubMed: 22975376]
37. Ros S, et al. Functional metabolic screen identifies 6-phosphofructo-2-kinase/fructose-2,6-biphosphatase 4 as an important regulator of prostate cancer cell survival. Cancer discovery. 2012; 2:328–343. [PubMed: 22576210]
38. Fan Q, et al. Akt and autophagy cooperate to promote survival of drug-resistance glioma. Science Signal. 2010; 3:ra81.
39. Fiedler T, et al. Arginine deprivation by arginine deiminase of Streptococcus pyogenes controls primary glioblastoma growth in vitro and in vivo. Can. Biol. Ther. 2015; 16:1047–55.
40. Shirwany NA, Zou MH. AMPK: a cellular metabolic and redox sensor. A minireview. Front Biosci. 2014; 19:447–74.
41. Jeon SM, Chandel NS, Hay N. AMPK regulates NADPH homeostasis to promote tumour cell survival during energy stress. Nature. 2012; 485:661–665. [PubMed: 22660331]
42. Denko NC. Hypoxia, HIF1 and glucose metabolism in the solid tumour. Nature reviews. Cancer. 2008; 8:705–713. [PubMed: 19143055]
43. Liu W, Shen SM, Zhao XY, Chen GQ. Targeted genes and interacting proteins of hypoxia inducible factor-1. Int J Bioche Mol Biol. 2012; 3:165–178.
44. Benita Y, et al. An integrative genomics approach identifies Hypoxia Inducible Factor-1 (HIF-1)-target genes that form the core response to hypoxia. Nucleic acids research. 2009; 37:4587–4602. [PubMed: 19491311]
45. Kelly DP, Scarpulla RC. Transcriptional regulatory circuits controlling mitochondrial biogenesis and function. Genes & development. 2004; 18:357–368. [PubMed: 15004004]
46. Bruni F, Polosa PL, Gadaleta MN, Cantatore P, Roberti M. Nuclear respiratory factor 2 induces the expression of many but not all human proteins acting in mitochondrial DNA transcription and replication. The Journal of biological chemistry. 2010; 285:3939–3948. [PubMed: 19951946]
47. Larsson NG, et al. Mitochondrial transcription factor A is necessary for mtDNA maintenance and embryogenesis in mice. Nature genetics. 1998; 18:231–236. [PubMed: 9500544]
48. Cantó C, Gerhart-Hines Z, Feige JN, Lagouge M, Noriega L, Milne JC, Elliott PJ, Puigserver P, Auwerx J. AMPK regulates energy expenditure by modulating NAD+ metabolism and SIRT1 activity. Nature. 2009; 458:1056–60. [PubMed: 19262508]
49. Levesque MJ, Raj A. Single-chromosome transcriptional profiling reveals chromosomal gene expression regulation. Nature methods. 2013; 10:246–248. [PubMed: 23416756]
50. Selak MA, et al. Succinate links TCA cycle dysfucntion to oncogenesis by inhibiting HIF-alpha prolyl hydroxylases. Cancer Cell. 2005; 1:77–85.
51. Kaelin WG. The Von Hippel-Lindau tumor suppressor protein: O2 sensing and cancer. Nat Rev Cancer. 2008; 8:865–873. [PubMed: 18923434]
52. Seidel S, et al. A hypoxic niche regulates glioblastoma stem cells through hypoxia inducible factor 2 alpha. Brain. 2010; 133:983–95. [PubMed: 20375133]
53. Dickinson A, et al. The regulation of mitochondrial copy number in glioblastoma cells. Cell Death Diff. 2013; 20:1644–53.
54. Sakamoto K, et al. Deficiency of LKB1 in skeletal muscle prevents AMPK activation and glucose uptake during contraction. The EMBO journal. 2005; 24:1810–1820. [PubMed: 15889149]

55. Thomson DM, et al. Skeletal muscle and heart LKB1 deficiency causes decreased voluntary running and reduced muscle mitochondrial marker enzyme expression in mice. American journal of physiology. Endocrinology and metabolism. 2007; 292:E196–202. [PubMed: 16926377]
56. McGee SL, Hargreaves M. AMPK-mediated regulation of transcription in skeletal muscle. Clinical science. 2010; 118:507–518. [PubMed: 20088830]
57. Thomson DM, et al. AMP-activated protein kinase phosphorylates transcription factors of the CREB family. Journal of applied physiology. 2008; 104:429–438. [PubMed: 18063805]
58. Li Y, Cummings RT, Cunningham BR, Chen Y, Zhou G. Homogeneous assays for adenosine 5'-monophosphate-activated protein kinase. Analytical biochemistry. 2003; 321:151–156. [PubMed: 14511678]
59. Mayr B, Montminy M. Transcriptional regulation by the phosphorylation-dependent factor CREB. Nature reviews. Molecular cell biology. 2001; 2:599–609. [PubMed: 11483993]
60. Jang T, et al. 5'-AMP-activated protein kinase activity is elevated early during primary brain tumor development in the rat. Int. J. Cancer. 2011; 128:2230–39. [PubMed: 20635388]
61. Ferreira D, et al. The Importance of Cancer Cell Lines as in vitro Models in Cancer Methylome Analysis and Anticancer Drugs Testing. Oncogenomics and Cancer Proteomics – in Chaves et al., "Novel Approaches in Biomarkers Discovery and Therapeutic Targets in Cancer". Chapter 6.
62. Rios M, et al. Lipoprotein internalisation induced by oncogenic AMPK activation is essential to maintain glioblastoma cell growth. Eur J Cancer. 2014; 50:3187–97. [PubMed: 25450947]
63. Saito Y, Chapple RH, Lin A, Kitano A, Nakada D. AMPK Protects Leukemia-Initiating Cells in Myeloid Leukemias from Metabolic Stress in the Bone Marrow. Cell Stem Cell. 2015; 17:585–96. [PubMed: 26440282]
64. Mo JS, et al. Cellular energy stress induces AMPK-mediated regulation of YAP and the Hippo pathway. Nat Cell Biol. 2015; 17:500–10. [PubMed: 25751140]
65. Liu X, et al. LncRNA NBR2 engages a metabolic checkpoint by regulating AMPK under energy stress. Nat Cell biol. 2016; 18:431–42. [PubMed: 26999735]
66. Papandreu I, et al. HIF-1 mediates adaptation to hypoxia by actively downregulating mitochondrial oxygen consumption. Cell Metab. 2006; 3:187–97. [PubMed: 16517406]
67. Dasgupta B, Milbrandt J. AMP-activated protein kinase phosphorylates retinoblastoma protein to control mammalian brain development. Dev. Cell. 2009; 16:256–70. [PubMed: 19217427]
68. Pooya S, et al. The tumour suppressor LKB1 regulates myelination through mitochondrial metabolism. Nat. Comm. 2014; 5:4993.
69. Komurov K, Dursun S, Erdin S, Ram PT. NetWalker: a contextual network analysis tool for functional genomics. BMC genomics. 2012; 13:282. [PubMed: 22732065]
70. Ernst J, et al. Mapping and analysis of chromatin state dynamics in nine human cell types. Nature. 2011; 473:43–9. [PubMed: 21441907]

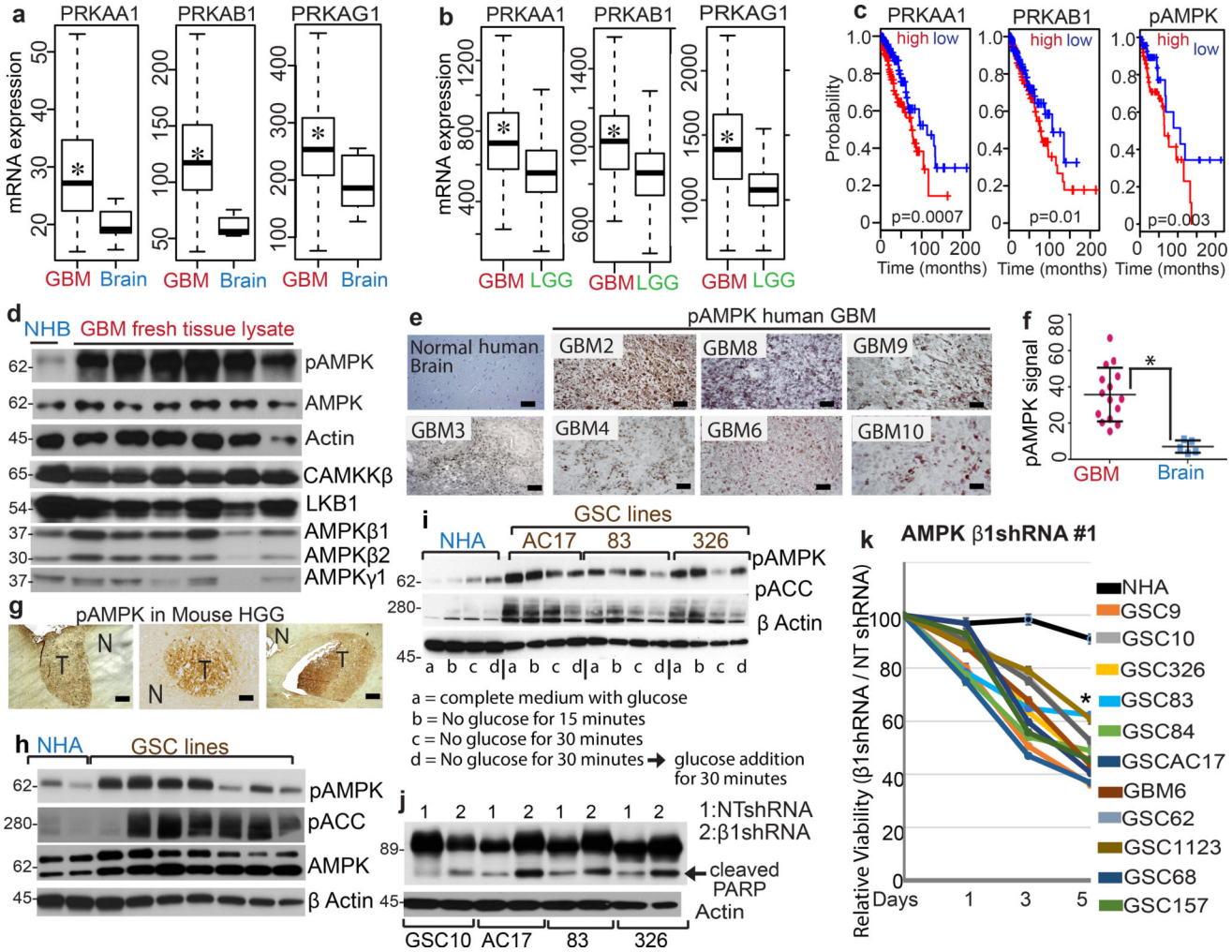

Figure 1. AMPK is highly expressed in GBM

a, b, Box plots (derived from TCGA Affimetrix data) showing high expression of AMPK isoforms in GBM compared to normal brain and low grade glioma (LGG). (n = 10 normal adult human brain versus 548 GBM and 534 LGG). The edges on the boxplots indicate the first and 3rd quartile (25th– and 75th percentile) of the data, with the line in the middle being the median. The whiskers on the boxplots extend another 1.5x of the inter-quartile range (between 25%–75% range of data) from the edges of the boxes, respectively. **c**, Kaplan-Meier survival plots of LGG patients. **d.** Western blot (WB) showing levels of pAMPK and AMPK pathway genes in GBM and normal human brain. **e**, Immunohistochemical analysis (IHC) of normal brain and GBM using pAMPK antibody. Scale bar 100μm. **f**, quantitation of pAMPK signal in human tissues (n = 15 GBM; 5 normal brain). * p= 0.0005. **g**, IHC showing pAMPK signal in mouse high grade glioma; N = normal tissue; T = tumor. Scale bar 500μm. **h**, WB of pAMPK and pACC in primary human GSC lines and normal human astrocytes (NHA). **i**, WB showing pAMPK and pACC in NHA and GSC lines in response to changes in glucose concentration. **j**, WB using PARP1 antibody showing cleaved PARP in control and AMPKβ1 shRNA expressing GSCs. Actin was used as a loading control. **k**, Viability of GCSs and NHA expressing nontarget or AMPKβ1 shRNA. (n = 3 independent

experiments). *p < 0.005. Error bars represent S.D ± mean. Statistical significance in above experiments was assessed using Student's two-tailed t-test, except (a, b) where Welch's t test was used. Source data are available in Supplementary Table 4. All WB represent data from 2–3 independent repeats. Unprocessed blots in Supplementary Fig. 9.

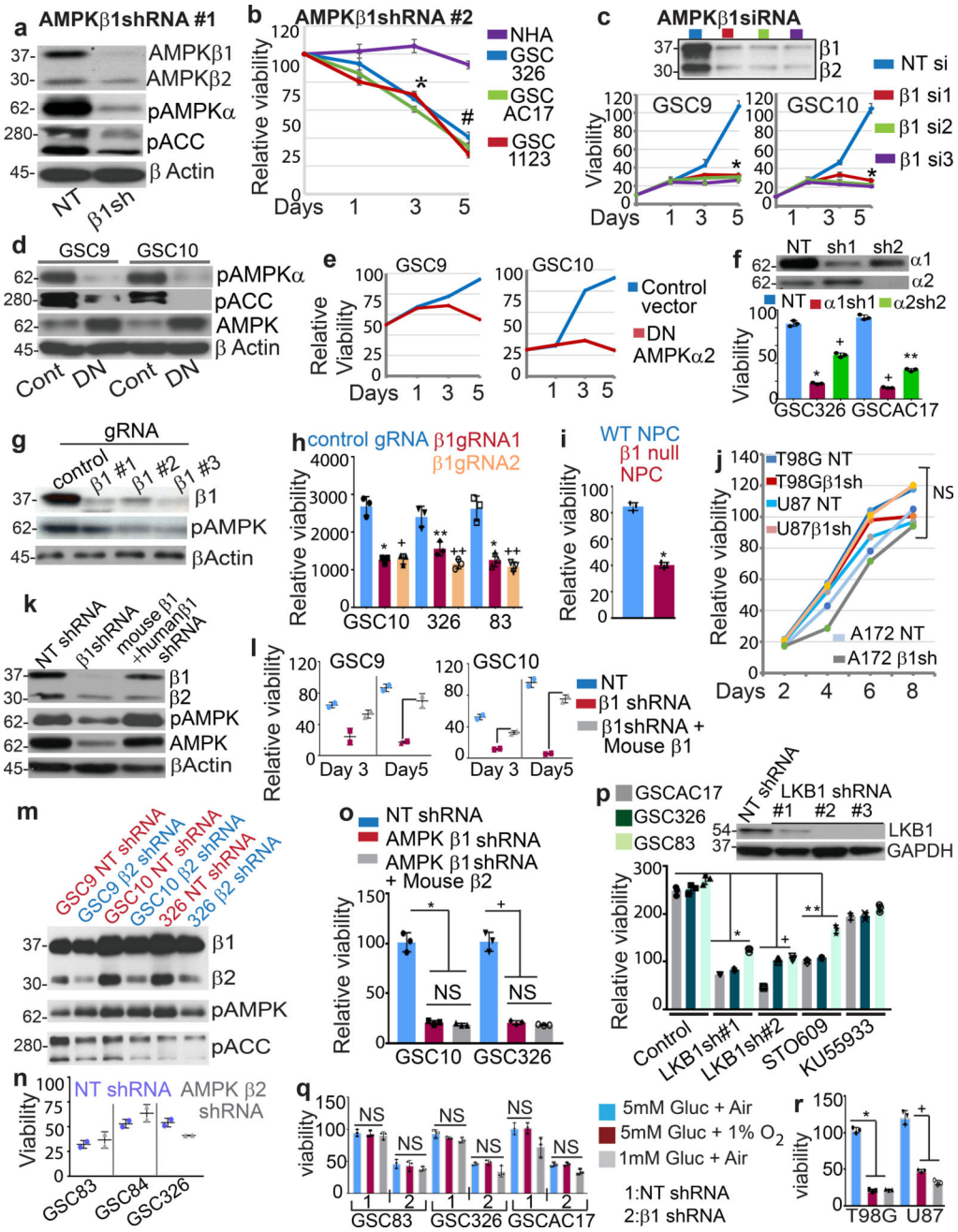

Figure 2. AMPK is essential for viability of primary GBM lines in vitro

a, WB using pAMPK, pACC and AMPKβ1/β2 common antibody in AMPKβ1shRNA treated GSC10. **b**, Cell viability using AMPKβ1 shRNA#2. (n=3). *p ≤ 0.007; # ≤ 0.001. **c**, GSC viability using AMPKβ1 siRNA. (n=3). *p ≤ 0.001. Inset: Western blot of β1/β2. Note: due to sequence homology, siRNAs knocked down both β1 and β2. **d**, WB of pAMPK and pACC in GSC lines expressing dominant negative (DN) AMPKα2. **e**, GSC viability using DN AMPK (Average of two independent experiments). **f**, GSC viability using AMPKα1/α2 shRNA. (n =3). * P = 0.0004; +0.0002, **0.0003. Inset: WB of AMPKα1/α2. **g**, WB showing CRISPR knockout of AMPKβ1 in GSC10. **h**, Viability of GSCs expressing

AMPKβ1 CRISPR. (n =3). Note: CRISPR transfection efficiency in GSCs is low (~ 30–40%). *p = 0.004, $^{+}$0.002, **0.01, $^{++}$≤ 0.006. **i**, Viability of oncogenic mouse neural stem cells (NPC) from compound floxed mice (Ink4/Arf−/−; Pten lox/lox with AMPKβ1lox/lox or AMPKβ1+/+) treated with Adeno-Cre. (n =3). *p = 0.0006. **j**, Viability of established GBM serum cell lines expressing AMPKβ1 shRNA (Average of two independent experiments). **k**, WB of GSC10 expressing human AMPKβ1 shRNA with or without mouse AMPKβ1. Note: AMPK α1/2 subunits are unstable in the absence of β subunits. **l**, Viability of GSCs expressing human AMPKβ1 shRNA with or without mouse AMPKβ1. (Average of two independent experiments). **m**, WB in GSCs expressing AMPKβ2 shRNA. **n**, GSC viability in the presence of AMPKβ2 shRNA. (Average of two independent experiments)). **o**, Viability of GSCs expressing human AMPKβ1 shRNA with or without mouse AMPKβ2. (n =3). *p ≤ 0.003, $^{+}$≤0.004; NS = nonsignificant. **p**, Viability of GSCs expressing LKB1 shRNA or treated with CAMKKβ inhibitor (STO) or ATM inhibitor (KU). (n =3). *p ≤ 0.0008; $^{+}$0.0004; **0.0006. Inset: WB showing efficiency of LKB1 shRNA. **q, r**, Viability of GSCs or GBM serum lines at indicated conditions. (n =3). NS = nonsignificant; *p ≤ 0.0006; $^{+}$≤ 0.003. Error bars; mean +/− S.D. Statistical significance; two-tailed t-test. n values are independent experiments Source data are available in Supplementary Table 4. WB represent data from 2 (d, g, k, m, p) or-3 (a, c) independent repeats. Unprocessed blots in Supplementary Fig. 9.

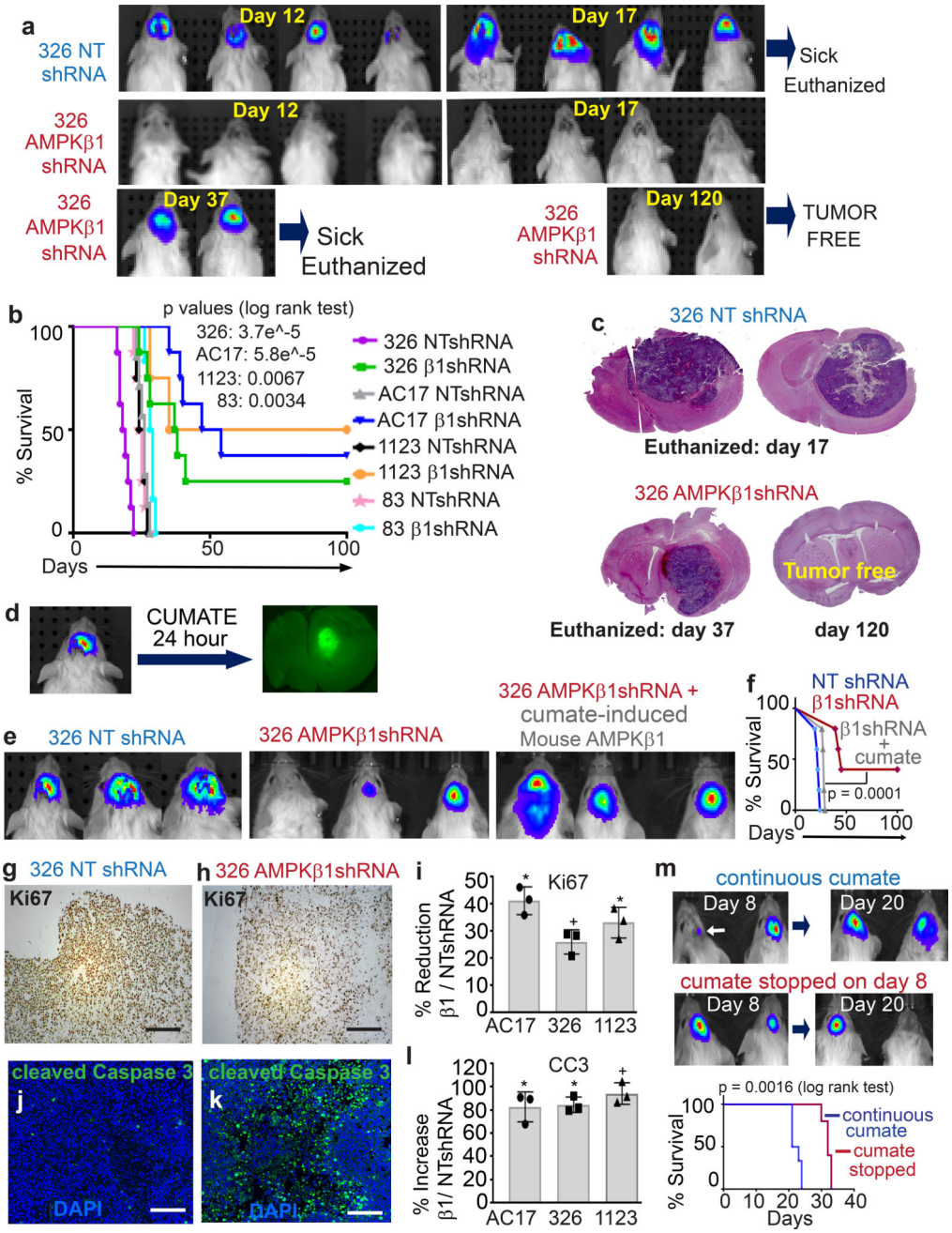

Figure 3. AMPK is essential for optimal GSC growth in vivo

a, Luciferase imaging of mice to monitor tumor growth of a GSC line expressing AMPKβ1 or nontarget (NT) shRNA at indicated days. n= 8 mice per group (4 shown). **b**, Kaplan-Meier survival data of four GSC lines expressing NT or AMPKβ1 shRNA. Note: the difference in survival between line 83 NTshRNA and 83 β1shRNA is not apparent due to the extended X axis, but is still significant. [n: 326 (8 NT and 8 β1shRNA); AC17 (7 NT and 8 β1shRNA); 1123 (4 NT and 4 β1shRNA; 83 (8 NT and 6 β1shRNA)] **c**, Hematoxylin and Eosin (H&E) staining of tumors harvested at indicated days. **d–f**, *In vivo* specificity of AMPKβ1 shRNA was tested by using a cumate-inducible lentiviral expression system. The

system works through the CymR repressor that binds the cumate operator sequences with high affinity. The repression is alleviated through the addition of Cumate, a non-toxic small molecule that binds to CymR. **d**, GSC326 transduced with cumate-inducible lentivirus and luciferase lentivirus were transplanted intracranially. Following confirmation of tumor growth by luciferase imaging, intraperitoneal delivery of water-soluble cumate (150 mg/kg) rapidly turned on GFP. **e**, GSC326 expressing cumate-inducible mouse AMPKβ1 were transduced with human AMPKβ1 shRNA or NT shRNA and transplanted intracranially. 50% mice with AMPKβ1 shRNA received cumate or vehicle once every day. The images shown were captured on day 17 post transplantation. **f**, Kaplan-Meier survival data of three groups (n = 5 mice per group). p = 0.0001. **g, h**, IHC of Ki67 in NT and AMPKβ1 shRNA expressing tumors. Scale bar 100μm. **i**, Quantification of Ki67 positive cells. (n = 3 mice/line/genotype). *p ≤ 0.001, $^{+}$≤0.004. **j, k**, IHC of cleaved Caspase 3 in NT and AMPKβ1 shRNA expressing tumors. Nuclei were stained with DAPI. Scale bar 100μm. **l**, Quantification of cleaved Caspase 3 positive cells. (n = 3 mice/line/genotype). *p ≤ 0.02, $^{+}$≤0.002. **m**, Tumors were established using GSC326 line expressing cumate-inducible mouse AMPKβ1 and human AMPKβ1 shRNA. Once tumors formed, cumate induction was continued in one group and stopped in another group. Kaplan-Meier survival data was plotted on two groups of mice (n = 5 – 6 mice / condition). Error bars; mean +/− S.D. Statistical significance; two-tailed t-test. Source data are available in Supplementary Table 4.

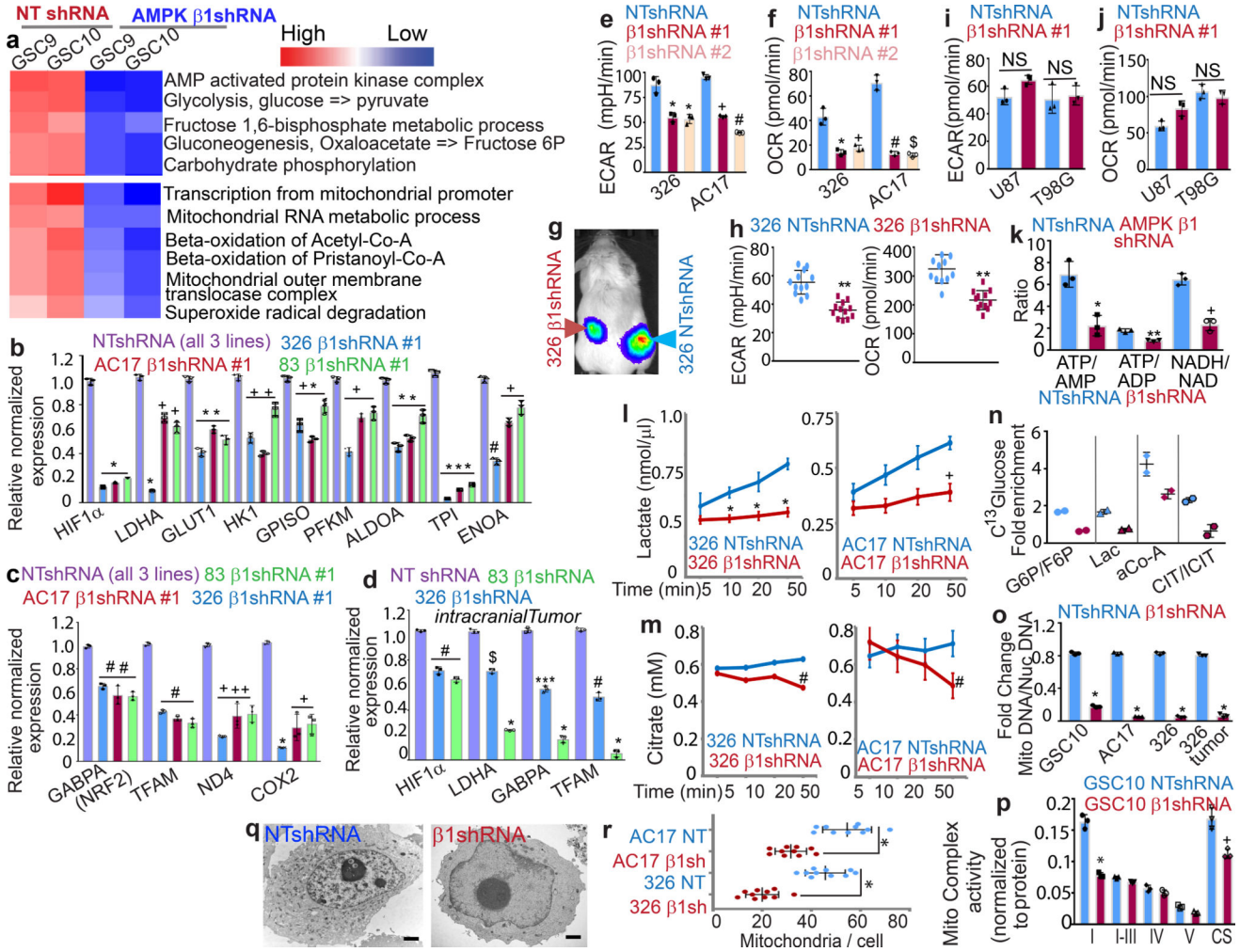

Figure 4. AMPK regulates GBM bioenergetics

a, Edge Flux heat map showing pathways downregulated in AMPKβ1 shRNA expressing GSCs. Data was processed through NetWalker. **b–d**, Relative expression of selective genes using Q-RTPCR in GSCs (b, c) or tumors (d) expressing nontarget (NT) or AMPKβ1 shRNA. Data was normalized to β-Actin. (n = 3). *p ≤ 0.0003; $^{+}$ ≤ 0.006; ** ≤ 0.003; $^{++}$ ≤ 0.005; $^{+*}$ ≤ 0.01; *** ≤ 0.0002; $^{\#}$ = 0.001; $^{\#\#}$ ≤ 0.009; $^{+++}$ ≤ 0.008. **e–j;** ECAR (extracellular acidification rate, a measure of glycolysis), and OCR (oxygen consumption rate, a function of mitochondria) of GSCs (e, f), flank tumors (g, h) and established GBM serum lines (i, j) expressing NT or AMPKβ1 shRNA. (n = 3) in e, f, i, j, and (n = 12 tumors/genotype) in g, h. *p = 0.003, $^{+}$0.0008, $^{\#}$0.0004 in 2e; *p = 0.008, $^{+}$0.0008, $^{\#}$0.001, $^{\$}$0.001 in 2f; **p ≤ 0.0001 in h. NS = nonsignificant in i, j. **k**, HPLC/Mass spectrometric quantification of cellular energy levels in GSC10 line expressing NT or AMPKβ1 shRNA. *p = 0.03; **0.01; $^{+}$0.001. (n = 3). **l, m**, Lactate and citrate released in media by GSCs expressing NT or AMPKβ1shRNA. (n = 3) *p = 0.01; $^{+}$0.03; $^{\#}$ ≤ 0.005. **n**, kinetic flux analysis of $U^{13}C$ glucose by HPLC/Mass-spec in GSCs expressing NT or AMPKβ1shRNA. (Average of two independent experiments) **o**, Quantification of mitochondrial mass in GSCs expressing NT or AMPKβ1shRNA by PCR using β-actin and ND4 primers. (n = 3). *p ≤ 0.0007. **p**,

Quantification of mitochondrial complex activity in GSCs expressing NT or AMPKβ1shRNA. (n = 3). *p = 0.003; $^{+}$0.01. **q**, Electron micrographs of GSC326 expressing NT or AMPKβ1shRNA. Scale bar 2μm. **r**, Quantification of mitochondrial number in 2 GSC lines expressing NT or AMPKβ1shRNA. (n = 10 cells /condition). **p ≤ 0.0002. Error bars: mean +/− S.D. Statistical significance; two-tailed t-test. n values represent independent experiments unless stated otherwise. Source data are available in Supplementary Table 4.

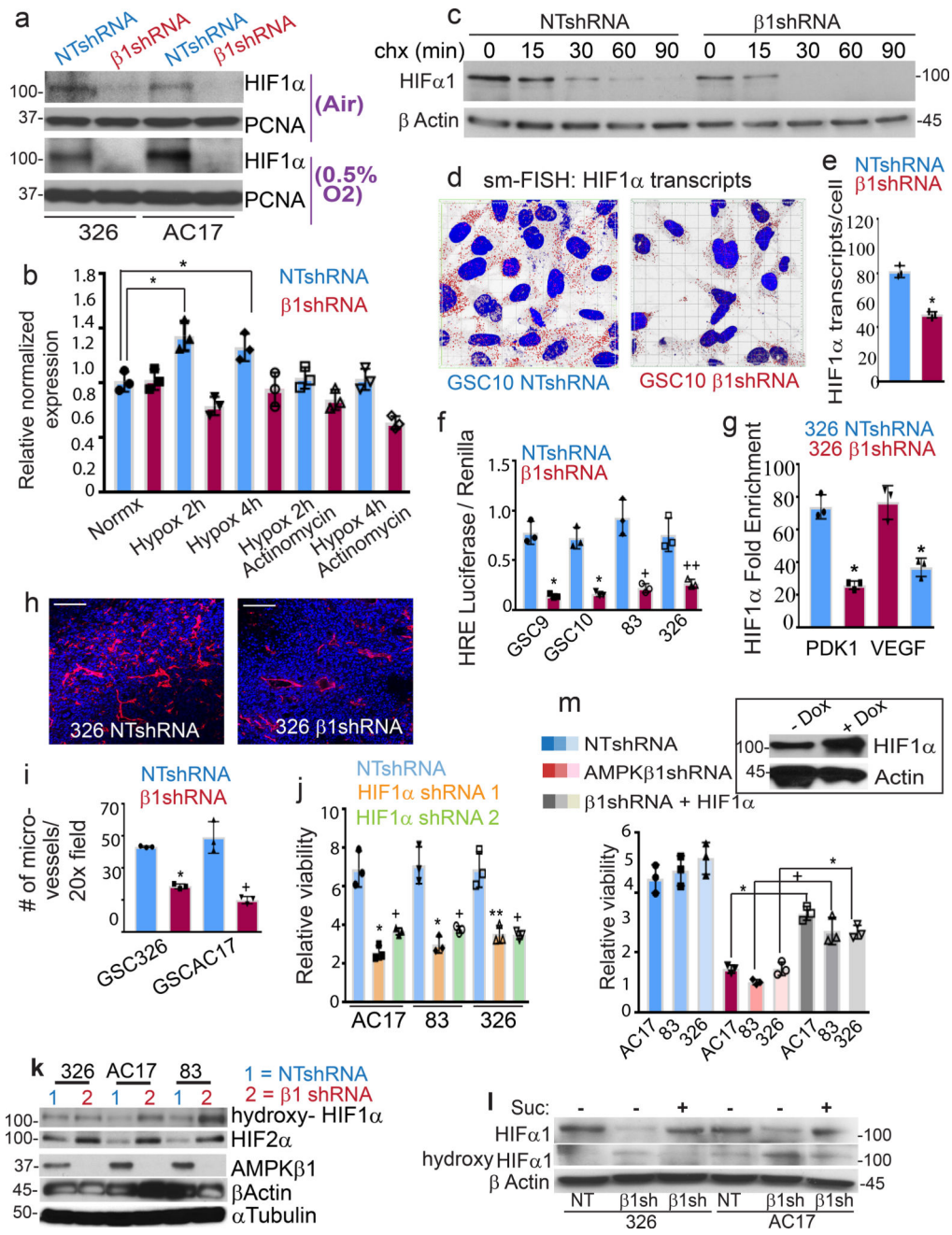

Figure 5. AMPK regulates HIF1α transcription in GSCs

a, WB of HIF1α in GSCs expressing NT or AMPKβ1 shRNA. PCNA was used as loading control. **b**, Quantification of HIF1α transcript in Actinomycin D-treated GSCs expressing NT or AMPKβ1 shRNA. Data was normalized to HPRT RNA. (n = 3). *p ≤ 0.003. **c**, WB of HIF1α in Cycloheximide-treated GSCs expressing NT or AMPKβ1 shRNA. **d**, Small molecule FISH (sm-FISH) coupled with high content imaging of nascent HIF1α transcripts in GSCs expressing NT or AMPKβ1 shRNA. **e**, Quantification of HIF1α RNA in sm-FISH. (n = 3). *p = 0.001. **f**, Quantification of HIF1α promoter activity in control (NT) and AMPK-silenced GSCs expressing hypoxia responsive element (HRE)-firefly and renilla

luciferase reporters. (n = 3). * p = 0.007; $^{+}$0.01; $^{++}$0.02. **g**, Chromatin immunoprecipitation (ChIP) using ChIP-grade HIF1α antibody and quantification of HIF1α binding to target gene promoters in control (NT) and AMPK-silenced GSCs. (n = 3). *p = 0.005. **h, i**, Microvascular density in AMPK silenced tumors using Isolectin B4 IHC (h) and quantification (i) in NT and AMPKβ1 shRNA expressing GSC326. (n = 3 tumors/genotype). Scale bar = 100μM. *p= 0.002; $^{+}$0.01. **j**, Viability of GSCs expressing NT or HIF1α shRNAs. (n = 3). *p ≤ 0.005; $^{+}$0.02; **0.007. **k, l**, WB of hydroxylated HIF1α, HIF1α and HIF2α in NT and AMPKβ1 silenced GSCs (k) and cells treated with 1mM succinate (l). **m**, Viability of NT or AMPKβ1 shRNA GSCs overexpressing dox-inducible constitutively active HIF1α. (n = 3). *p ≤ 0.0004; $^{+}$0.01. Inset: WB of HIF1α in control (-dox) and dox-treated cells. Error bars; mean +/− S.D. Statistical significance; two-tailed t-test. N means biological replicates. Source data are available in Supplementary Table 4. All WB represent data from 2 (c,k, i) or 3 (a, m) independent repeats. Unprocessed blots in Supplementary Fig. 9.

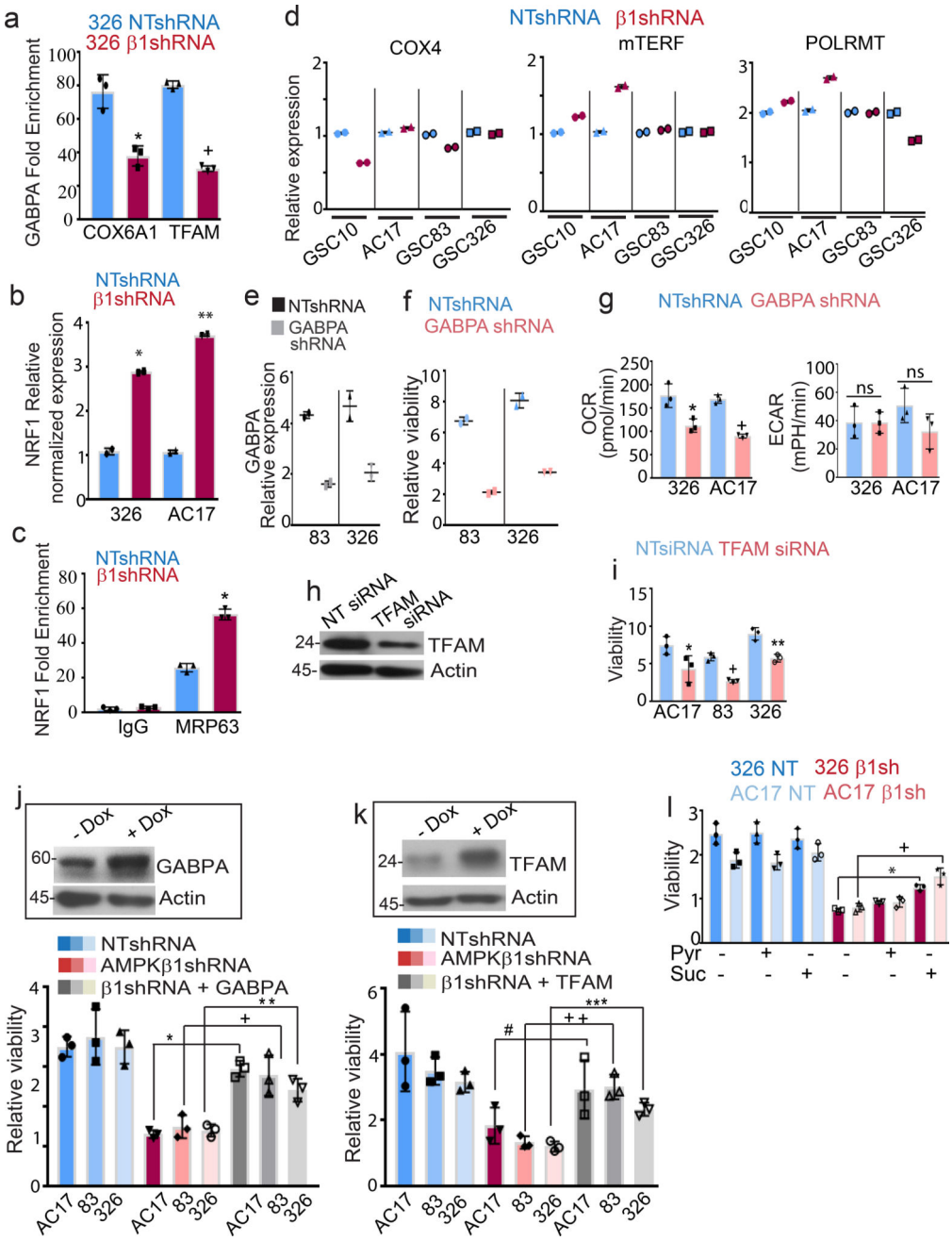

Figure 6. AMPK regulates GABPA transcription in GSCs

(a), ChIP using GABPA antibody and quantification of GABPA binding to target gene promoters in control (NT) and AMPK-silenced GSCs. (n = 3). *p = 0.003; $^{+}$0.001. **b**, Q-RTPCR analysis of NRF1 in GSCs expressing NT or AMPKβ1 shRNA. (n = 3). *p = 0.006; **0.005. Data was normalized to β actin. **c**, ChIP using NRF1 antibody or nonspecific IgG and quantification of NRF1 binding to target gene promoters in NT and AMPKβ1 shRNA-expressing cells. (n = 3). *p = 0.003. **d**, Q-RTPCR analysis of COX4, mTERF and POLRMT in NT and AMPKβ1 silenced GSC lines. (Average of two independent experiments). **e,f**, Q-RTPCR of GABPA (e) and cell viability (f) in GSCs expressing NT or

GABPA shRNA. (Average of two independent experiments). **g**, OCR and ECAR in GSCs expressing GABPA shRNA. (n = 3). *p = 0.009; $^{+}$0.001; ns = nonsignificant. **h, i**, WB of TFAM (h) and cell viability (i) in GSCs expressing NT or TFAM siRNA. (n = 3). *p = 0.01; $^{+}$0.002, **0.003. **j, k**,. Viability of NT or AMPKβ1-expressing GSCs overexpressing GABPA (j) or TFAM (k). Insets: WB of GABPA (j) and TFAM (k) with or without Dox treatment. (n = 3). *p ≤ 0.001; $^{+}$=0.009; **p =0.005; $^{\#}$0.03; $^{++}$0.004; ***0.0008. **I**, Viability of NT or AMPKβ1shRNA-expressing GSCs treated with methylpyruvate (1mM) or sodium succinate (1mM). (n = 3). *p = 0.001; $^{+}$0.006. Error bars: mean +/− S.D. Statistical significance; two-tailed t-test. n values represent independent experiments. Source data are available in Supplementary Table 4. Western blots represent data from 2 (h, j) or 3 (k) independent repeats. Unprocessed blots in Supplementary Fig. 9.

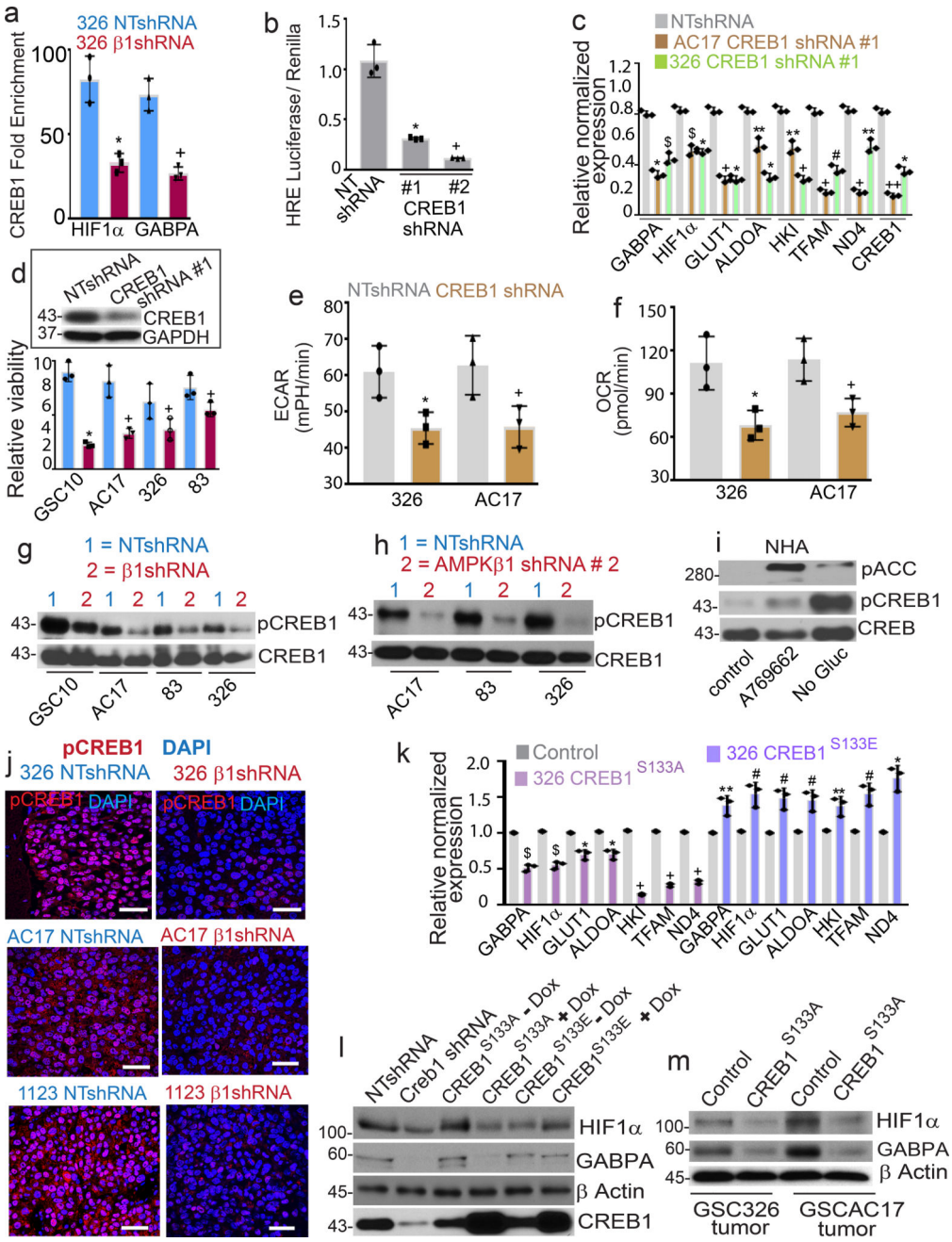

Figure 7. AMPK regulates HIF1α and GABPA through CREB1

a, ChIP using CREB1 antibody and quantitative PCR showing CREB1 binding to promoter/enhancer regions of HIF1α and GABPA. (n = 3). *p = 0.009; $^{+}$0.005. **b**, Quantification of HIF1α promoter activity in control (NT) and CREB1-silenced GSCs expressing HRE-firefly and renilla luciferase reporter plasmids. (n = 3). * p = 0.01. $^{+}$ 0.008. **c**, Q-RTPCR analysis of GSCs expressing NT or CREB1 shRNA. (n = 3). *p = 0.002; $^{+}$ 0.001; # 0.004; $^{\$}$0.007; **0.01; $^{++}$0.0005. **d**, Viability of GSCs expressing NT or CREB1 shRNA. (n = 3). *p = 0.003; $^{+}$0.01. Inset: WB of CREB1. **e, f**, ECAR and OCR in GSCs expressing CREB1 shRNA. (n = 3). *p = 0.01; $^{+}$0.006. **g, h**, WB of pCREB1^{S133} and CREB1 (loading control)

in GSCs expressing NTshRNA or two independent AMPKβ1shRNA. **i**, WB of pACC, pCREB1 and CREB1 in normal human astrocytes (NHA) treated with AMPK activator A769662 or glucose starvation (30 min). **j**, IHC of $pCREB^{S133}$ in tumors derived from GSCs expressing NT or AMPKβ1 shRNA. Scale bar 100μm. **k**, Q-RTPCR analysis of GSC 326 expressing control virus, $CREB1^{S133A}$, or $CREB1^{S133E}$ lentivirus. (n = 3). *p = 0.01; $^{+}\leq$ 0.0003; $^{\$}$0.002; $^{\#}$0.02; **0.03. **I**, WB of HIF1α and GABPA in GSCs expressing CREB1 shRNA, $CREB1^{S133A}$ and $CREB1^{S133E}$ mutants. Total CREB1 and actin are also shown. **m**, WB of HIF1α and GABPA in tumors derived from GSCs expressing^{S133A}. Error bars; mean +/− S.D. Statistical significance; two-tailed t-test. N values represent independent experiments. Source data are available in Supplementary Table 4. All western blots represent data from 2 (I, l, m) or 3 (g, h) independent repeats. Unprocessed blots are shown in Supplementary Fig. 9.

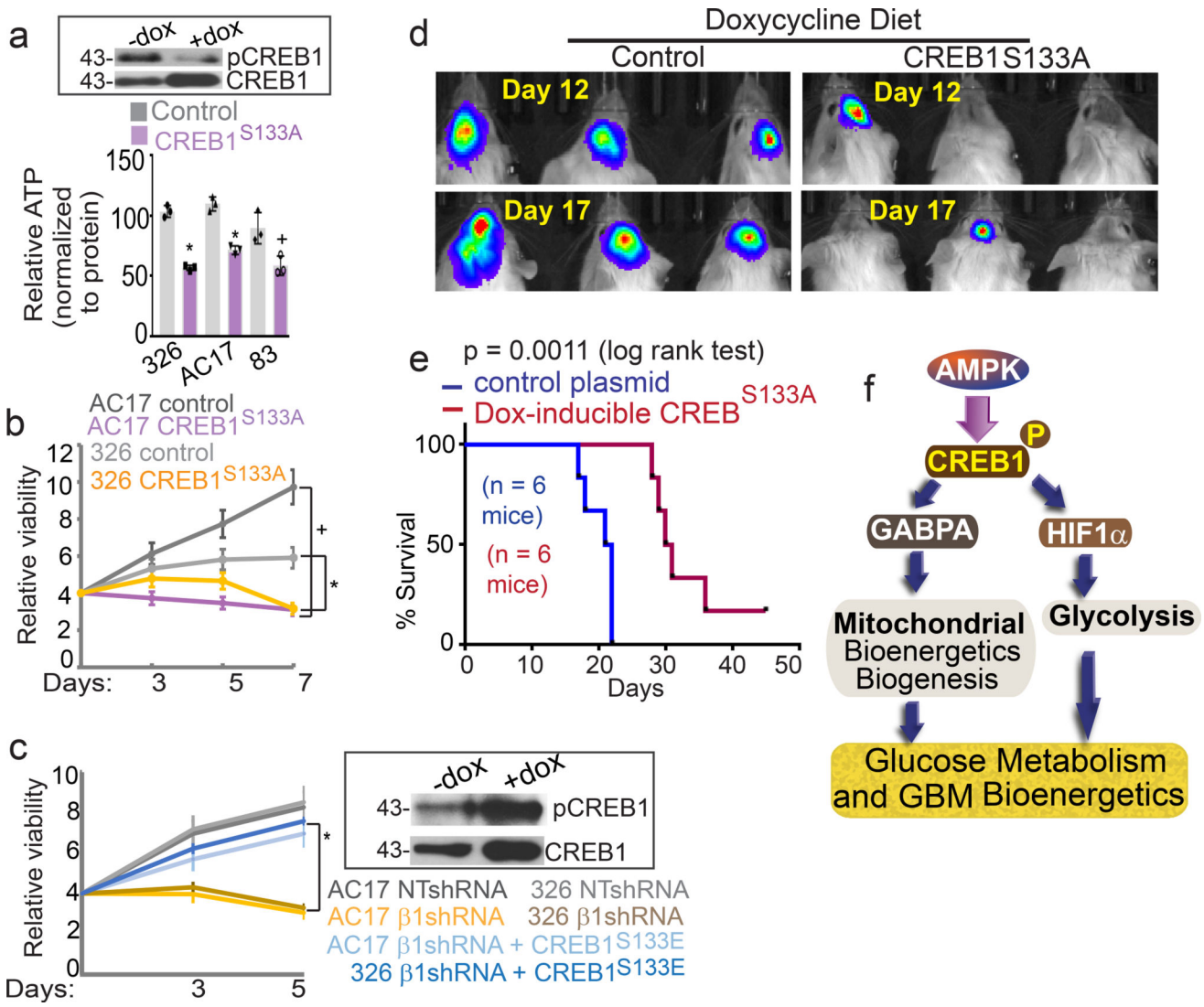

Figure 8. AMPK-CREB1 transcriptional axis regulates GBM bioenergetics and tumor growth

a, ATP levels in GSCs expressing CREB1^{S133A} mutant. (n = 3). *p = 0.001; $^{+}$ 0.008. Inset: WB of pCREB1 and CREB1 in GSCs expressing dox-inducible CREB1^{S133A} in the presence or absence of dox. **b**, Viability of GSCs expressing CREB1^{S133A} or control virus. (n = 3). * P = 0.002; $^{+}$ 0.005. **c**, Viability of GSCs expressing NT or AMPKβ1shRNA and overexpressing CREB1^{S133E}. (n = 3). * P ≤ 0.002. Inset: WB of pCREB1 and CREB1 in GSCs expressing dox-inducible CREB1^{S133E} in the presence or absence of dox. **d**, Growth of tumors expressing control virus or dox-inducible CREB^{S133A} in NSG mice fed with dox-chow after tumor establishment. **e**, Kaplan-Meier survival data of dox diet-fed mice with tumors expressing control virus or dox-inducible CREB^{S133A}. (n = 6 mice / condition). **f**, Schematic showing the regulation of GBM bioenergetics by AMPK. AMPK phosphorylates CREB at serine 133. This allows enhanced binding of CREB1 to its targets namely HIF1α and GABPA. HIF1α and GABPA in turn augment the transcriptional program of glycolysis and mitochondrial biogenesis to regulate GBM viability and growth. Error bars: mean +/− S.D. Statistical significance in above experiments (except e) was assessed using two-tailed t-

test. N values represent independent experiments. Source data are available in Supplementary Table 4. All western blots represent data from 2 (a, c) independent repeats. Unprocessed blots are shown in Supplementary Fig. 9.